Forschungszentrum Karlsruhe
Technik und Umwelt
Wissenschaftliche Berichte
FZKA 5629

Measurement of the Fuel Temperature and the Fuel-to-Coolant Heat Transfer Coefficient of Super Phénix 1 Fuel Elements

M. Edelmann

Institut für Neutronenphysik und Reaktortechnik
Projekt Nukleare Sicherheitsforschung

Dezember 1995

Forschungszentrum Karlsruhe
Technik und Umwelt
Wissenschaftliche Berichte
FZKA 5629

Measurement of the Fuel Temperature and the Fuel-to-Coolant Heat Transfer Coefficient of Super Phénix 1 Fuel Elements

M. Edelmann
Institut für Neutronenphysik und Reaktortechnik
Projekt Nukleare Sicherheitsforschung

Forschungszentrum Karlsruhe GmbH, Karlsruhe
1995

Als Manuskript gedruckt

Forschungszentrum Karlsruhe GmbH
Postfach 3640, 76021 Karlsruhe

ISSN 0947-8620

Messung der Brennstofftemperatur und der Wärmeübergangszahl Brennstoff-Kühlmittel der Super-Phénix1-Brennelemente

Zusammenfassung

Es wird berichtet über eine neue Meßmethode zur Bestimmung der mittleren Brennstofftemperatur und der Wärmeübergangszahl zwischen Brennstoff und Kühlmittel in den Brennelementen (BE) eines Natrium-gekühlten schnellen Brutreaktors. Die Methode beruht auf einer individuellen BE-Wärmebilanz bei Reaktorschnellschluß. Die Methode wurde mit Erfolg am französischen Brüter-Prototyp SPX1 eingesetzt.

Die mittlere Brennstofftemperatur im BE als auch die Wärmeübergangszahl wurden für stationären Reaktorbetrieb bei 15 bis 90% Nennleistung und 3 bis 83 Vollasttagen Abbrand für alle BE des SPX1 bestimmt. Die Messungen lieferten jeweils auch die Zeitkonstanten der Brennstoffzone sowie des gesamten BE. Die Genauigkeit der gemessenen BE-Parameter wird auf 10% geschätzt.

Brennstofftemperaturen und BE-Austrittstemperaturtransienten wurden zum Vergleich auch mit dem SPX1-Projektcode DYN2 für jeweils gleichen Brennstoff- und Reaktorbetriebszustand wie im Experiment berechnet. Die gemessenen Brennstofftemperaturen waren in allen Fällen höher als die gerechneten. Die Differenz zwischen gemessenen und gerechneten Core-Mittelwerten beträgt 50K bei niedriger Leistung und steigt auf 180K bei 90% NL. Das entspricht etwa der doppelten Meßunsicherheit. Die gemessenen Wärmeübergangszahlen sind etwa 20% kleiner als die entsprechenden Wärmeübergangsparameter der Rechnung.

Unterschiede zwischen gemessenen und gerechneten Temperaturtransienten lassen vermuten, daß entweder der transiente Wärmeübergang im Spalt zwischen Brennstoff und Brennstabhülle im Rechenmodell nicht richtig reproduziert wird oder daß die Spaltweite im frischen Brennstoff schon größer war als in der Rechnung vorausgesetzt.

Measurement of the Fuel Temperature and the Fuel-to-Coolant Heat Transfer Coefficient of Super Phénix 1 Fuel Elements

Summary

A new measurement method for measuring the mean fuel temperature as well as the fuel-to-coolant heat transfer coefficient of fast breeder reactor subassemblies (SA) is reported. The method is based on the individual heat balance of fuel SA's after fast reactor shut-downs and uses only the plants normal SA outlet temperature and neutron power signals. The method was used successfully at the french breeder prototype Super Phenix 1.

The mean SA fuel temperature as well as the heat transfer coefficient of all SPX SA's have been determined at power levels between 15 and 90% of nominal power and increasing fuel burn-up from 3 to 83 EFPD (Equivalent of Full Power-Days). The measurements also provided fuel and whole SA time constants. The estimated accuracy of measured fuel parameters is in the order of 10%.

Fuel temperatures and SA outlet temperature transients were also calculated with the SPX1 systems code DYN2 for exactly the same fuel and reactor operating parameters as in the experiments. Measured fuel temperatures were higher than calculated ones in all cases. The difference between measured and calculated core mean values increases from 50 K at low power to 180 K at 90% n.p. This is about the double of the experimental error margins. Measured SA heat transfer coefficients are by nearly 20% lower than corresponding heat transfer parameters used in the calculations.

Discrepancies found between measured and calculated results also indicate that either the transient heat transfer in the gap between fuel and cladding (gap conductance) might not be exactly reproduced in the computer code or that the gap in the fresh fuel was larger than assumed in the calculations.

CONTENTS

I - INTRODUCTION

The fuel temperature as well as the heat transfer coefficient between fuel and coolant of fast reactor subassemblies are important parameters in reactor dynamics calculations and safety analyses.

The fuel temperature at nominal operating conditions is also an essential design parameter of nuclear reactors. It depends on fuel pin geometry and thermal conductivities of the fuel and fuel-clad interspace, for instance. The exact values of these parameters in turn are depending on the fuel fabrication process as well as on reactor operating conditions and fuel burn-up. Thus, they are changing during the core fuel cycle.

Neither the initial values nor the change of heat transfer parameters of a fuel element can be predicted with very good precision. This is true especially for the fuel-clad gap conductance which is the most uncertain of these parameters.

In an operating power reactor the fuel temperature of a SA is not accessible to direct measurement. It can only be calculated from SA power and coolant temperature. Precise calculations of the fuel temperature and related reactivity feedback effects as, for instance, axial fuel expansion or Doppler effect require a good estimate of the heat transfer coefficient between fuel and coolant. Presently, rather large uncertainties of thermal fuel parameters have to be taken into account in calculating the fuel temperature and reactivity effects depending thereon.

Therefore, an experimental programme was run at the French fast power reactor SUPER PHENIX 1 which aimed at measuring the heat transfer coefficient and the fuel temperature of individual fuel elements and their dependance on reactor operating conditions and fuel burn-up.

For this purpose a new measurement method had to be developed which enables to determine these parameters within the error limits of about 10 % in order to reduce existing uncertainties. Previously developed and successfully tested methods [1] using noise analysis techniques do not work at SPX1 because of insufficient correlation between power and outlet temperature fluctuations [2]. For this reason fairly large and fast power transients are required for the measurement of thermal fuel element parameters. The new method is based on measuring the heat released from the fuel after a fast reactor shut-down. In this way the fuel temperature and heat transfer coefficient for the previous operating conditions can be obtained.

This is an advantage over an earlier method in which fuel time constants were derived from the outlet temperature response to power transients by fitting model-predicted temperatures [3, 4]. These time constants can be used to check reactor dynamics calculations and thermal fuel parameters used in them. However, the heat transfer coefficient which can be derived thereof does not correspond to the operating conditions before the transient. Rather, it characterizes the transient heat transfer between the initial and final reactor state. During large power transients the thermal conductivities and heat capacities which determine the fuel time constant may change significantly with temperatures. Then the dynamic fuel time constant would not give the initial values of fuel temperature and heat transfer coefficient.

The new method also yields the fuel time constant for the SA power before the shut-down. This is an interesting parameter of a fuel element. Because it is not only the response time of the outlet temperature to power perturbations. It gives at the same time the heat content of the SA in units of SA power. However, at SPX1 the fuel elements include as an integral part the upper axial neutron shield (PNS - protection neutronique supérieure). This is a

long thick-walled steel tube which together with the upper blanket represents a large thermal buffer. Variations of coolant temperature can be significantly modified between the fuel pin bundle and SA exits. This concerns the thermal response time of the SA as well as its heat content. These effects and also the transmission characteristics of the thermocouple (TC) at the SA outlet on measured temperatures are dealt with and taken into account in the analysis of the measurements.

The start-up procedure of the SUPER PHENIX reactor provided for the first time the opportunity to extensively study the thermal fuel performance of a very large number of fast reactor subassemblies. During the approach to full power there was a certain number of scheduled and incidental reactor scrams from various stationary power levels with increasing fuel burn-up. At these occasions the outlet temperatures of 469 SA positions are automatically recorded by the core surveillance system CORA [5]. In the first core only 358 of them were loaded with fuel elements. The others were breeder elements (72), dummies (18) and control rods (21). These recordings, called fast perturbographies, cover the time span from 50 s before to 60 s (optional 120 s) after the triggering event.

From the CORA perturbographies and neutron power and other auxiliary signals measured separately with the experimental SA surveillance system KASUMOS [6] the fuel and SA time constants, over-all heat transfer coefficients and mean fuel temperatures of all fuel SA's have been determined. The measurements cover power levels from 15 % to 90 % of nominal power and fuel burn-up between 4 and 83 EFPD's.

For the evaluation of the measurements a special computer programme was written. It provides listings and coloured core maps of various SA parameters including time constants, heat transfer coefficients and fuel temperatures. Although originally written for KASUMOS it could be easily adapted to run on other HP mini-computers as those available at the SSAE of C.E.N. Cadarache or at the SPX1 power plant at Creys-Malville.

II - PRINCIPLE AND BASIC EQUATIONS OF THE MEASUREMENT METHOD

The principle of the method consists of measuring the change of the thermal energy of the fuel in a SA between two different levels of reactor and SA power. If the fuel temperature in the final state is known as for instance, after reactor shut-down, the initial fuel temperature can be obtained from a simple heat balance. As mentioned before this heat balance has to include the upper breeder blanket and neutron shield.

Figure 1 shows the main components of the SPX1 SA in a schematic cross-section. It was shown earlier [7] that the fuel pin bundle to a good approximation can be described by a simple lumped-parameter model. The same should be true for the blanket and neutron shield. All of them can be considered as a solid mass interacting with a flowing coolant at a different temperature. This also holds for the thermocouple (TC), at the SA outlet. The whole system, will therefore be modeled by a series of three lumped-parameter models of the same type which interact successively with the coolant stream. The first section represents the fuel region, the second one includes blanket and PNS whereas the last one models the thermocouple.

Inputs to the first section are coolant inlet temperature and SA power. For the other sections the input is equal to the outlet temperature of the preceding one. The first section differs from the others mainly by the fact that there is a temperature difference between solid and fluid even at stationary operation due to the power generated in the fuel. Each section is completely defined by only six parameters. These are : heat capacity and mean temperature of solid and fluid, an over-all heat transfer coefficient between them and the power generated in the solid. The power generated in the last sections is negligible compared to the power generated in the fuel. Therefore, only the fuel section model equations will be solved. The solutions for the others are obtained by setting the power equal to zero.

The heat balance for the fuel and the coolant within the fuel section is described by the two coupled differential equations

$$C_f \dot{T}_f(t) = P(t) - k(T_f(t) - T_c(t)) \qquad (1)$$

$$C_c \dot{T}_c(t) = k(T_f(t) - T_c(t)) - 2hF(T_c(t) - T_i(t)) + C_c \dot{T}_i(t)) \qquad (2)$$

with :

T_f	mean temperature of fuel
$T_c = \frac{T_o + T_i}{2}$	mean coolant temperature
T_i, T_o	inlet and outlet temperature
C_f, C_c	heat capacity of fuel and coolant
P	subassembly power
k	overall heat transfer coefficient between fuel and coolant
h	specific heat of coolant
F	coolant flow rate

Equs. (1), (2) can be written in the equivalent form

$$C_f \dot{T}_f(t) = P(t) - k(T_f(t) - T_i(t)) + k(T_c(t) - T_i(t)) \qquad (1')$$

$$C_c \dot{T}_c(t) = k(T_f(t) - T_i(t)) - (k + 2hF)\,(T_c(t) - T_i(t)) + C_c \dot{T}_i(t)) \qquad (2')$$

For stationary operating conditions we have at $t \leq 0$

$$\dot{T}_i(t) = \dot{T}_c(t) = \dot{T}_f(t) = 0 \tag{3}$$

and

$$T_i(t) = T_i^\circ,\ T_c(t) = T_c^\circ,\ T_f(t) = T_f^\circ,$$

$$P(t) = P^\circ = 2hF(T_c^\circ - T_i^\circ) = hF(T_o^\circ - T_i^\circ) \tag{4}$$

From equ. (2') it follows then

$$T_c^\circ - T_i^\circ = \gamma\ (T_f^\circ - T_i^\circ) \tag{5}$$

where the parameter γ is defined as

$$\gamma = \frac{k}{k + 2hF} \tag{6}$$

This is an important heat transfer parameter. It gives the ratio of the temperature rises of coolant and fuel :

$$\gamma = \frac{T_c^\circ - T_i^\circ}{T_f^\circ - T_i^\circ} = \frac{\Delta T_c^\circ}{2\ \Delta T_f^\circ} \tag{7}$$

with

$$\Delta T_c = T_o - T_i = 2(T_c - T_i) \tag{8}$$

Now we define

$$\tau_f = \frac{C_f}{k} \tag{9}$$

which will turn out to be the fuel time constant [s]. Then we obtain from equations (1), (1') and (6) :

$$\tau_f P^\circ = C_f(T_f^\circ - T_c^\circ) = (1 - \gamma) C_f(T_f^\circ - T_i^\circ) \quad (10)$$

or

$$C_f(T_f^\circ - T_i^\circ) = \tau_1 P^\circ \quad (11)$$

where

$$\tau_1 = \frac{\tau_f}{1 - \gamma} = \tau_f + \frac{C_f}{2hF} \quad (12)$$

According to equ. (11) τ_1 gives the heat in power units being stored in the fuel. That means that τ_1 seconds of the SA power are stored as heat energy in the fuel. It will be shown later that τ_1 is also the response time of the coolant temperature to power variations. Thus, there are two possibilities to determine the fuel time constant τ_f.

This was done earlier by directly measuring the dynamic response of coolant outlet temperatures to power variations using noise analysis or power perturbations techniques [1, 3]. Another method would consist of measuring the total heat removed from the SA after a fast reactor shut-down and using equs. (10) or (11) and (12) to determine the fuel time constant. Then the heat transfer coefficient and the fuel temperature can be calculated with equs. (9) and (1), respectively. It seems that this is the first time that thermal dynamics fuel parameters have been measured in this way. Both methods have been used at SPX1 and will be discussed in detail.

For this purpose equs. (1) and (2) will be solved explicitely. This can be easily done by using Laplace transforms. To illustrate this procedure we will determine the transfer function of the TC at the SA outlet from equ. (1).

The Laplace transform of a function Y(t) is defined as

$$y(s) = \int_0^\infty \exp(-st)\, Y(t)\, dt = \mathcal{L}\{Y(t)\} \qquad (13)$$

with the complex Laplace variable $s = x + j\omega$, $j^2 = -1$. From equ. (13) we obtain immediatly the useful relationship

$$y(0) = \int_0^\infty Y(t)\, dt \qquad (14)$$

which will be used later in heat balance calculations. It should be mentioned also here that for $s = j\omega$ and $\omega = 2\pi f$ a representation of the model equations in the frequency domain is obtained.

For the TC we have $P(t) \equiv 0$ and $T_f^\circ = T_c^\circ$ where T_f in this case denotes the TC temperature.

With the TC time constant τ defined according to equ. (9) equation (1) reads

$$\tau\, \dot{T}_f(t) + T_f(t) = T_c(t)$$

Its Laplace transform is

$$(1 + \tau s)\, T_f(s) = T_c(s) + \tau T_c^\circ$$

Thus, for the TC temperature we have the equation

$$T_f(s) = K(s)\, (T_c(s) + \tau\, T_c^\circ) \qquad (15)$$

with

$$K(s) = \frac{1}{1 + \tau s} \qquad (16)$$

For $s = j\omega$ equ. (16) represents the TC transfer function which corresponds to a simple low-pass filter characteristics with the cut-off frequency $f_c = 1/2\pi\tau$. Coolant temperatures at higher than this frequencies are filtered-out by the TC. For frequencies $f << f_c$ the TC causes a pure time delay of the temperature variation. This is true because for $|s| << 1/\tau$ the transfer function can be approximated by

$$K(s) = \frac{1}{1 + \tau s} \approx \frac{1}{1 + \tau s + (\tau s)^2/2 + \ldots} = \frac{1}{\exp(\tau s)}$$

$$= \exp(-\tau s) \qquad (17)$$

which in the time domain represents a pure time shift of τ.

The exact equivalent of K(s) in the time domain, i.e. the impulse response or Green's function is

$$K(t) = \frac{1}{\tau} \exp(-t/\tau) \qquad (18)$$

from which the step response function follows by integration :

$$\int_0^t K(x)\, dx = 1 - \exp(-t/\tau) \qquad (19)$$

This is the response to a positive unity step. The response of the TC to the inverse step from 1 to zero would be

$$U(t) = \exp(-t/\tau) \qquad (20)$$

Integrating this function gives the time constant.

According to equ. (14) this result can be obtained directly from equ. (15) for $T_c^*(s) \equiv 0$ and $T_c^* = 1$ because $K(s = 0) = 1$.

From equs. (18) and (20) it is seen that $\tau K(t)$ is equal to the (negative) step response. Consequently, the second term in equ. (15) represents the TC response to a coolant temperature step from T_c° to zero. Thus, the total temperature signal consists of a superposition of the low-pass filtered coolant temperature and the exponential decay of the initial temperature at t = 0 (step response). The integral (14) over the temperature signal is larger than the integral over the temperature itself :

$$T_f\ (s = 0) = T_c\ (s = 0) + \tau\ T_c^\circ \tag{21}$$

In this work we are mainly interested in coolant temperature variations produced by changes of reactor power. These are slow with respect to the TC time constant. Thus, the main effects of the TC will be a time shift (17) and an increase (21) of the integral of coolant temperature.

The solution of equs. (1), (2) for the fuel section with constant heat capacities and heat transfer coefficient is given in appendix A. For the mean coolant temperature within the fuel section one obtains

$$T_c(s) = H(s)\ \frac{P(s)}{2hF} + H_i(s)\ T_i(s)$$

$$+ \frac{H(s)}{b}\ [(s + a)\ T_c^\circ + \dot{T}_c^\circ - (s + b\tau_f)\ T_i^\circ - \dot{T}_i^\circ] \tag{22}$$

wherein the power and inlet temperature transfer functions are defined respectively as

$$H(s) = \frac{1 - \gamma}{(1 + \tau_f s)\ (1 + \tau_c s) - \gamma} \tag{23}$$

$$H_i(s) = 1 - \frac{C_f + C_c}{2hF}\ sH(s) \tag{24}$$

with :

$$\tau_c = \gamma \frac{C_c}{k} = \frac{C_c}{k + 2hF} \tag{25}$$

$$a = \frac{\tau_f + \tau_c}{\tau_f \tau_c} \tag{26}$$

$$b = \frac{1 - \gamma}{\tau_f \tau_c} \tag{27}$$

The power-to-coolant temperature transfer function (23) represents a second-order low-pass characteristics with feedback.

The thermal feedback mechanism of the coolant temperature on the heat flux between fuel and coolant and on the fuel temperature is rather complicated. This can be seen in a block diagram shown in [7] (Fig. 3). It cannot be described by a single parameter. However, it follows from equ. (1') that in some way γ could be taken as measure of this feedback. With increasing coolant flow rate both γ and the coolant temperature rise ΔT_c are decreasing. The heat flux out of the fuel is equal to $k(\Delta T_f - \Delta T_c)$. Thus, the coolant temperature rise decreases the heat sink in equ. (1'). To provide the removal of the heat produced in the fuel the fuel temperature must increase. This leads to an increase of the coolant response time (fuel time constant) which is determined by the feedback parameter γ as will be seen further down.

For $\gamma = 0$ (no feedback) the transfer function (23) is composed of two first-order low-pass characteristics as defined in equ. (16). The corresponding Green's function consists therefore of two exponentials with the time constants τ_f and τ_c, respectively. The second time constant (25) is called the coolant time constant because it depends on the coolant heat capacity whereas the fuel time constant (9) is determined by the heat capacity of the fuel.

For a finite coolant flow rate, which means heat transfer with thermal feedback, equ. (23) is written in the form

$$H(s) = \frac{b}{s^2 + a\,s + b} = \frac{qr}{(s - q)\,(s - r)} \tag{28}$$

wherein q and r represent the roots of the equation

$$s^2 + a\,S + b = 0$$

$$q,\ r = -\frac{a}{2} \pm \sqrt{\frac{a^2}{4} - b} \tag{29}$$

With the definitions

$$\tau_1 = -\frac{1}{q} \tag{30}$$

$$\tau_2 = -\frac{1}{r} \tag{31}$$

the power transfer function (23), (28) reads

$$H(s) = \frac{1}{(1 + \tau_1 s)\,(1 + \tau_2 s)} \tag{32}$$

which corresponds to a second-order low-pass without feedback but with different time constants.

For the SA parameters of SPX1 given in Tab. I the modified time constants can be calculated to a very good approximation using the following formulas (Appendix A).

$$\tau_1 = \frac{a}{b} - \frac{1}{a} \approx \frac{\tau_f}{1 - \gamma} \tag{33}$$

$$\tau_2 = \frac{1}{a} \approx \left(1 - \frac{\tau_c}{\tau_f}\right) \tau_c \tag{34}$$

These time constants will be called fuel and coolant response time of the coolant temperature, respectively. The thermal feedback increases the fuel response time and decreases the coolant response time. Especially at low coolant flow the difference is significant for the first one as can be seen from Tab. I.

The inlet-to-outlet temperature transfer function (24) represents a band rejection characteristics because s.H(s) disappears for large frequencies and for s = 0. For the fuel section this transfer function is of minor interest because the inlet temperature variations in this kind of experiments are small and fairly slow. Thus, they can be neglected in most cases. However, for the upper neutron shield (PNS-section) of the SA this is different. There we have large coolant temperature variations which are significantly modified by this transfer function as will be seen later.

For practical applications it is convenient to replace the mean coolant temperature T_c by the coolant temperature rise (8) and using the change of inlet temperature

$$\delta T_i(t) = T_i(t) - T_i^\circ$$

$$\delta T_i(s) = T_i(s) - \frac{T_i^\circ}{s} \qquad (35)$$

instead of the inlet temperature itself. For stationary initial operating conditions (3), (4) we obtain instead of equ. (22) :

$$\Delta T_c(s) = H(s)\ \left(\frac{P(s)}{hF} + \frac{s + a}{b}\ \Delta T_c^\circ - Q_1 s\ \delta T_i(s)\right) \qquad (36)$$

$$\text{where } Q_1 = \frac{C_f + C_c}{hF} \qquad (37)$$

For the measurement of SA time constants the normalized temperature rise

$$\Delta N(s) = \Delta T_c(s)/\Delta T_c^\circ \tag{38}$$

and the corresponding equation

$$\Delta N(s) = H(s)\ \left(\frac{P(s)}{P^\circ} + \frac{s + a}{b} - Q_1\ s\ \frac{\delta T_i(s)}{\Delta T_c^\circ}\right) \tag{39}$$

are used. In this way signal calibration factors for SA power and temperature rise are eliminated. The last term in (39) represents the first derivative of the inlet temperature

$$s\delta T_i(s) = \dot{\delta T}_i(s)$$

The integral (14) over the normalized temperature rise in the fuel section follows directly from equ. (39) :

$$\Delta N\ (s = 0) = \frac{\tau_f + \tau_c}{1 - \gamma} + \frac{P(s = 0)}{P^\circ} - Q_1\ \frac{\delta T_i(t)}{\Delta T_c^\circ} \tag{40}$$

This is the basic equation of the new measurement method. Thus, a reactor scram provides directly the sum of the response times of the fuel section

$$\tau_1 + \tau_2 = \frac{\tau_f + \tau_c}{1 - \gamma} \tag{41}$$

because $P \equiv 0$ for $t > 0$ and $\delta T_i << \Delta T_c^\circ$ for $t < 6\ \tau_1$. In case of a non-ideal power step or non-negligible inlet temperature variations the normalized power integral and inlet temperature variation $Q_1\ (T_i^\circ - T_i(t))/\Delta T_c^\circ$ have to be subtracted from the normalized temperature rise integral.

According to equs. (4), (40), (41) the heat removed from the fuel section after a power step from P° to zero is

$$hF\ \Delta T_c^\circ\ \Delta N_s(s = 0) = P^\circ(\tau_1 + \tau_2) \tag{42}$$

Since it was shown earlier (equ. (11)) that $\tau_1\ P^\circ$ represents the heat stored in the fuel before the power step the second term

$$\tau_2\ P^\circ = C_c\ (T_c^\circ - T_i^\circ) = C_c \Delta T_c^\circ/2 \tag{43}$$

must be the heat stored in the coolant and cladding of the fuel section.

For a perfect power step equ. (39) reads

$$\Delta N_s(s) = \frac{s + a}{b} H(s) \tag{44}$$

The inverse Laplace transform of equ. (44) gives the step response function in the time domain

$$\Delta N_s(t) = \frac{1}{\tau_1 - \tau_2} \left(\tau_1 \exp\left(-\frac{t}{\tau_1}\right) - \tau_2 \exp\left(-\frac{t}{\tau_2}\right)\right) \tag{45}$$

which for SPX1 and similar fuel elements (see time constants in Tab. I) can be sufficiently well approximated by

$$\Delta N_s(t) \approx \begin{cases} 1 \text{ for } t < \tau_2 \\ \exp\left(-\dfrac{t - \tau_2}{\tau_1}\right) \text{ for } t \geq \tau_2 \end{cases} \tag{46}$$

By fitting this equation or equ. (45) to a measured step response of SA outlet temperature both time constants can be determined separately. This does not require a fast reactor scram. The method can be also used with small power perturbations [1].

In principle, inherent power fluctuations can be also used to measure the transfer function $H(\omega)$ by noise analysis techniques.

But in general only the fuel response time τ_1 can be obtained from $H(\omega)$ by least-squares fitting equ. (32) to it. This results from the fact that the coolant response time is smaller than the fuel response time by at least one order of magnitude. Therefore, it determines only high-frequency noise components for which the signal-to-background ratio is low.

Figure 2 shows examples of calculated transfer functions H(f) and $H_i(f)$ using equs. (16), (23) and (24) with SPX1 SA parameters for 90 % p.n. given in Tab. I. Obviously, the spectral composition of outlet temperature variations is essentially determined by the power transfer function H(f) due to its very low cut-off frequency $f_c = 1/2\pi\tau_1 = 0{,}03$ Hz. The TC transfer function with $\tau = 0{,}5$ s as well as the PNS inlet temperature transfer function have practically no effect on the amplitude of power-induced coolant temperature variations.

However, they do produce a phase shift which causes a significant time delay of the temperature response to power perturbations. This is illustrated in Fig. 3 by calculated step response function using equs. (20), (45), (46), (53) and (54) with SPX1 SA parameters as before.

To obtain a rough idea of the effect of the blanket and PNS section on coolant outlet temperatures the equivalent of equ. (36) with appropriate parameters as listed in the correspondence table (Tab. II) can be used to calculate the temperature rise $\delta\Delta T$ in the blanket and PNS section. With $P(s) \equiv 0$, $\Delta T_c^\circ = 0$ and inlet temperature = $\Delta N(s)$ we obtain

$$\delta\Delta T(s) = - Q_2 \; s \; G(s) \; (\Delta N(s) - \frac{1}{s}) \qquad (47)$$

where

$$Q_2 = \frac{C_a + C}{hF} \qquad (37')$$

and G(s) second-order low-pass characteristics as H(s) but with different time constants.

According to equ. (8) we can also write

$$\delta\Delta T(s) = \Delta T(s) - \Delta N(s) = \Delta T(s) - \frac{1}{s} - (\Delta N(s) - \frac{1}{s}) \qquad (48)$$

From equs, (47) and (48) we obtain the inlet-to-outlet temperature tranfer function of the PNS section

$$H_a(s) = \frac{\Delta T(s) - \frac{1}{s}}{\Delta N(s) - \frac{1}{s}} = 1 - Q_2 \; s \; G(s) \qquad (49)$$

The total normalized temperature rise of the SA follows from equs. (39), (47) and (48) to be

$$\Delta T(s) = H(s) \; (\frac{P(s)}{P^\circ} + \frac{s + a}{b} - Q_1 \; s \; \frac{\delta T_i(s)}{\Delta T_c^\circ})$$

$$+ Q_2 \; G(s) \; H(s) \; (1 - \frac{s \; P(s)}{P^\circ} + Q_1 \; s^2 \; \frac{\delta T_i(s)}{\Delta T_c^\circ}) \qquad (50)$$

The gain $/ H_a(f) /$ of the transfer function (49) was calculated with different sets of time constants τ_3, τ_4. The corresponding curves are shown in Fig. 2 together with fuel section transfer functions. They indicate that the PNS section of the SPX1 SA acts as a band rejection filter for fuel section outlet temperature variations.

However, it has to be pointed out that the time constants of the PNS section are not known. Therefore, the real filter characteristics might be different from those shown in Fig. 2. Furthermore, the transient heat transfer in the PNS is very complicated and cannot at all be calculated exactly. The reason for this difficulty comes from the poor thermal conductivity of the stainless steel together with the large wall thickness of the PNS (5 cm).

As a consequence, the effective values of PNS heat capacity and heat transfer coefficient are changing during a coolant temperature transient. At the beginning heat is exchanged only with a thin layer close to the inner PNS surface. This means that the heat capacity is small whereas the heat transfer coefficient is fairly high. Thus, the initial time constant is very small. A decrease of coolant temperature would be quickly balanced out thus producing a delay of a temperature transient. Small temperature fluctuations might be more or less reduced depending on their amplitude and frequency range.

In a continued temperature transient heat is exchanged with layers more and more far from the surface which results in an increase of the time constant due to increasing thermal resistance and effective heat capacity. In the analysed SPX1 shut-down transients already 30 s after scram the temperature rise in the PNS was nearly constant (~ 1 K) although only 20 % of its initial heat were removed. This was found by time and space dependent numerical calculations with the reactor dynamics code DYN2 of C.E.N. Cadarache. These calculations will be reported in the next paragraph.

The PNS time constants have no influence on the temperature rise integral. The total heat removed from the SA including fuel and PNS section after reactor scram can be obtained from equ. (50) for $s = 0$ as for the fuel section alone, equ. (42) :

$$Q = (\tau_1 + \tau_2 + Q_2)\ P^\circ$$
$$= (\tau_1 + \tau_2)\ P^\circ + (C_a + C)\ \Delta T^\circ \qquad (51)$$

Thus, the additional heat released from the PNS section is equal to its total heat capacity multiplied by the initial coolant temperature rise. As mentioned before, in our measurements the effective PNS heat capacity is only a small fraction of its total value.

For a power step from P° to zero with constant inlet temperature equ. (50) becomes

$$\Delta T_s(s) = \Delta N_s(s) + Q_2\ G(s)\ H(s) \qquad (52)$$

The corresponding step response function in the time domain is composed of the fuel section step response (45), (46) and four additional exponentials according to the four time constants τ_1 to τ_4 in G(s) H(s). The exact total SA Step response function

$$\Delta T_s(t) = \Delta N_s(t) + Q_2\ \mathcal{L}^{-1}\ (\ G(s)\ H(s)\ ) \qquad (53)$$

as well as approximations of it are explicitely given in Appendix A. They are not so easy to interpret as the fuel section step response. At high coolant flow rates (Q_2 small) the PNS term in equ. (53) can be represented to a first approximation by an additional time delay of the fuel section step response (46).

$$\Delta T_s(t) = \begin{cases} 1 \text{ for } t < \tau_2 + Q_2 \\ \exp\left(-\dfrac{t - \tau_2 - Q_2}{\tau_1}\right) \text{ for } t \geq \tau_2 + Q_2 \end{cases} \qquad (54)$$

This indicates that the delay Q_2 of temperature variations in the PNS increases with decreasing coolant flow. For nominal flow we have $Q_2 \approx 0{,}8$ s but at 15 % of nominal flow this would be a delay of about 5 s. This delay does not include the coolant transit time.

In Fig. 3 various step response functions of fuel and PNS sections are plotted together to illustrate the effect of thermal feedback in the fuel section, heating in the PNS as well as the difference between exact and approximate solutions of the model equations. The agreement with measured step responses is fairly good as found already earlier [1]. This is true even for SPX1 SA's with integrated upper neutron shield [4]. Approximate step response functions agree even better than exact solutions with measured temperatures. This is due to the fact that constant mean PNS time constants are too large for sufficiently fast buffering of the initial part of the temperature transient.

We conclude that in principle the fuel time constant is modified only by the thermal feedback in the fuel section. Except for the first few seconds of the transient the PNS section produces only a time delay but does not significantly change the shape of the temperature transient from which the fuel response time (time constant) can still be determined. The same is true for the TC's at the SA outlets. They essentially cause a small time delay (17) corresponding to their response time. All of the three SA model sections are releasing heat after a power transient. The resulting normalized temperature integral over the transient is significantly increased by thermal feedback and heat exchange in the PNS section. This must be explicitely taken into account when fuel time constants are determined from post-scram heat removal of a SA.

The simple model developed here assumes constant heat capacities and transfer coefficients in fuel and PNS sections. However, these parameters depend on fuel and coolant temperatures which in turn are functions of SA power. Therefore, the results obtained in this paragraph apply to noise analysis and power perturbation techniques only where power variations are sufficiently small. For the accurate analysis of large power transients they might be used with corrections in some cases. This is true for the determination of fuel temperature and heat transfer coefficient by measuring the heat removal after reactor scram as will be seen later.

III - NUMERICAL CALCULATIONS OF POWER AND COOLANT TEMPERATURE TRANSIENTS

The numerical calculations were performed[1)] with the SPX1 system code DYN2 using consistent sets of reactor and fuel parameters (power, coolant flow, fuel burn-up, etc.) exactly representing the experimental conditions of the measurements.

DYN2 is a one-dimensional computer code which simulates the over-all performance of the whole power plant including core, primary sodium pool, heat exchangers, pumps secondary loops, steam generators and the feed water system. However, in our case only the primary system was calculated using measured inlet temperatures instead of calculated ones, the primary coolant flow being constant in the time interval of interest.

Core dynamics is simulated in DYN with four fissile and three fertile channels, each of them representing a group of sub-assemblies. Within a channel an average pin model is used to represent the axial distribution of power and material properties by a fine nodal structure including lower gas plenum and blanket, fuel, upper blanket and shield as well as SA head. The pin geometry is represented by concentric cylindrical radial fuel nodes, clad, coolant region and structural material.

For the stationary reactor operating conditions prior to the transient the fuel-to-coolant heat transfer was calculated with the code ASTROLAB2 which is based on fuel behaviour models taking into account fuel restructuration, swelling and creep phenomena as well as formation and release of fission gas according to the previous operating conditions and burn-up. The heat exchange across the gap includes radiation and conduction in the filling gas according to the actual gap geometry. During the transient the gap geometry is recalculated in each time step (0,1 s) from the differential expansion of clad and fuel pellet as determined by the corresponding temperatures.

1) successively by C. ESSIG, B. BERTHET, B. VALENTIN and M. MULET

Originally outlet temperature transients have been calculated to determine fuel time constants in the same way as from measured transients. Intercomparing calculated and measured time constants enables to check the modeling of the heat transfer as well as of heat transfer parameters used in the code. This is reported in a previous paper [4] for initial reactor power levels from 23 % to 80 % of nominal power and low burn-up. Experimental and theoretical results agreed fairly well in these cases.

In Fig. 4 DYN calculated coolant temperatures after reactor scram from 80 % n.p. are shown. The lowest and highest one of the three temperatures represent the coolant temperatures at the fuel-blanket interface and SA outlet, respectively. They are very similar to those obtained from the simple lumped-parameter fuel element model shown in Fig. 3. However, the DYN-calculated temperatures at the SA outlet are about 1 K higher than those at the exit of the fuel region. In the initial state this is due to the power generated by fast fission in the upper blanket. Later this is due to the coolant temperature rise in the PNS which is almost constant after the main transient. Subtracting 1 K from the upper curve gives the third one which represents the outlet temperature without temperature rise in the blanket and in the PNS after the transient.

Both effects are not taken into account in the lumped parameter model. Their contribution to the heat balance will be accounted for by subtracting the integral over the DYN-calculated temperature difference between fuel section and SA outlet from the measured outlet temperature integral. In this way the whole PNS contribution to the heat removed from the SA during the transient is eliminated. It is also seen that the heat exchange in the PNS causes a slight increase of the time constant besides of the time delay discussed in the previous paragraph.

Calculated temperature transients after reactor scram from 50 % an 80 % n.p. are plotted in Figs. 5 and 6, respectively with corresponding measured temperatures of a central SA (2831) for comparison. At 50 % n.p. calculated and measured transients agree very well. Both of them can be represented by an exponential function with nearly the same exponent. However, at 80 % n.p. calculated temperatures decrease faster than measured ones especially at the beginning of the transient. But about 3 s after scram both of them can still be described quite well by an exponential the time constants of them being slightly different, though.

At 90 % of nominal reactor power this is no longer true. Whereas the real transient did not change significantly with respect to 50 % and 80 % transients the calculated temperature decreases in a different way. It can no longer be approximated by an exponential function. This is the main reason for which the new measurement method was developed. The evolution of the calculated and measured outlet temperature transients with increasing reactor power and fuel burn-up is illustrated by Figs. 7 and 8, respectively.

In order to find an explanation for this phenomenon the fuel temperatures at 50 % and 90 % n.p. were looked into. The DYN calculations provided the fuel temperature transients for the eight radial nodes at two axial positions, i.e. core midplane and fuel-blanket boundary. In Fig. 9 the axial distribution of the fuel temperature in all of the radial nodes is shown. Obviously, the heat transfer around the core midplane is much better than elsewhere. The axial temperature profile of the outermost radial node is about the inverse of the power profile. This is due to the axial variation of the fuel-clad interspace. In the central part this gap is closed. It opens increasingly towards the ends of the fuel pin. This effect leads to a rather flat axial profile of the radially averaged fuel temperature, which favourites the lumped-parameter SA model described in the previous paragraph.

For two axial positions of the outermost radial node the transient fuel temperatures have been plotted together with some other temperatures. The curves shown in Fig. 10 represent the temperatures during the scram from 50 % n.p. In Fig. 11 the corresponding temperatures are shown for the scram at 90 % n.p.

Evidently, before the scram at 50 % n.p. the gap is open all along the fuel pin because the fuel temperature at the axial midpoint is much higher than at the end of the pin. Furthermore, the transients at both positions are very similar.

At 90 % n.p. the fuel temperature at the midplane decreases much faster immediately after the scram than later on. This indicates that the gap reopens shortly after the power drop. This can be interpreted as a discontinuity in the heat transfer between fuel and coolant. The disconnection of the clad from the fuel together with the low temperature of the outer fuel nodes in the central axial positions leads to a more rapid decrease of the coolant temperature at the beginning of the transient. Afterwards the heat transfer from the inner radial nodes increases the fuel surface temperature which in turn leads to a slower decrease of the coolant temperature.

Thus, the discrepancy between measured and calculated SA outlet temperature transients is directly related to the modeling of the gap between fuel and cladding as well as to the calculation of the thermal gap conductance. It might be that the thermal contact between fuel and clad is less perfect in reality than in the empirical fuel behaviour model used in the DYN2 code (ASTROLAB2). Another possible explanation could be a larger than

assumed width of the gap already in the fresh fuel pins. Than the length at which the gap closes at high power would be less than calculated. Into addition, this would decrease the overall heat transfer coefficient at any power level. From this a higher than calculated fuel temperature might be expected. As will be seen later the measured mean fuel temperatures were indeed always higher than those obtained by the calculation with DYN2.

The DYN calculations also provided the radial temperature profile at two axial mesh points of the PNS. The profile shown in Fig. 12 represents the temperature distribution which exists 40 s after the scram at 90 % n.p. At this time the heat exchange between PNS and coolant is quasi-stationary. The coolant temperature rise in the PNS of about 1 K is decreasing very slowly as shown before (Fig. 4). Nevertheless, only 20,2 % of the initial heat content ($C_a \Delta T°$) have been removed yet. This is due to the poor conductivity of stainless steel. Consequently, the effective PNS heat capacity to be taken into account in the after-scram heat balance is only about 20 % of its total value. For evaluating the measurements the effective heat capacity of the PNS section including the upper blanket is determined by integrating the difference between the coolant temperatures at the SA outlet and fuel-blanket interface as calculated with DYN2. In this way the additional heat produced by fast fission in the blanket is also taken into account. From the normalized temperature integral an average value of 44,5 KJ/K of the effective heat capacity is obtained (equ. 37'). It will be used in the evaluation of all of the measurements.

IV - MEASUREMENT PROCEDURE

Outlet temperature transients were measured during two types of fast reactor shut-down. In the first one ("AR" : Arrêt Rapide) all of the 21 control rods of the primary shut-down system are inserted simultaneously at maximum drive speed. In the second one ("AU" : Arrêt d'Urgence, scram) these rods plus three additional ones of the secondary shut-down system are dropped. Only in the

latter case the power transient can be approximated by a step function of about 0,4 s rise time (Fig. 4). In the first one it takes about 30 s to completely shut-down the reactor. At SPX1 small power steps produced by moving a single control rod are not suitable for measuring SA parameters. This can be seen from Fig. 13 where measured power transients of the three types are shown together with corresponding calculated temperature transients using equ. (39).

In Tab. III the reactor operating conditions and experimental parameters of all the measurements are listed.

The power transients were normally measured by one neutron chamber inside (BOUPHY) and below the reactor vessel, each. The SA outlet temperatures were obtained from Cr-Al thermocouples about 10 cm downstream of the SA outlets. For a fast reactor shut-down all of these temperatures are recorded automatically at an increased sampling rate (1/s) by the plant's core surveillance system CORA. These CORA records -called fast perturbography- provide one inlet temperature of each primary loop, their mean value and the temperature rise (ΔT) of 469 core positions from 50 s before to 60 s (optionally 120 s) after the event which triggers the safety system. Thus, CORA perturbographies consist of 111 or 171 records of 474 temperatures.

The temperatures are not sampled simultaneously. They are scanned successively within a time interval of 600 ms. Therefore, there is an uncertainty of up to $\pm$ 300 ms in the sampling time of individual TC's. The same uncertainty exists in the normalized temperature integral over the transient. This uncertainty is eliminated to a good approximation by linearly interpolating the individual sampling times between first and last sampled subassemblies. The precise sampling time within the 600 ms time interval cannot be determined due to the non-determimistic procedure of scanning SA outlet temperatures of CORA.

There is no neutron power signal in the fast perturbographies.

Therefore, from the CORA perturbography alone neither the precise moment of the shut-down nor the transient power integral can be determined. But both of them are needed for the after-scram heat balance measurement (equ. 50). It is known that the triggering event happened somewhere between the 51st and 52nd record. However, due to delays in the redundant digital safety system with 1 s cycle time the shut-down might occur seconds later. In the transients being analysed in this work it was always between the 53^{d} and 54^{th} record.

For the above reasons a neutron power and at least one SA outlet temperature signal had to be measured separately. This was done with the experimental SA surveillance system KASUMOS [6] which was originally installed at SPX1 for measuring SA heat transfer parameters by noise analysis techniques using temperature signals from intrinsic TC's at the SA outlets. As mentioned before this does not work at SPX1. The reasons for this are given in [2].

Although outlet temperature transients cannot be measured with SS-Na TC's due to their high-pass transmission characteristics their signal can be used to synchronize CORA and KASUMOS perturbographies (the Cr-Al TC's of the safety system are normally not accessible to direct measurement). KASUMOS provided digital records of in general three neutron power and eight SS-Na TC signals (analog) which are available from the plants on-line noise analysis system ANABEL [8]. The sampling rate was 18,8/s.

The way the CORA and KASUMOS perturbographies were synchronized is illustrated in Fig. 14. First of all a mixed data file of CORA and KASUMOS perturbographies is created in which CORA signals were interpolated to obtain the KASUMOS sampling interval. Signals of both data sets were roughly synchronized by properly choosing the starting point for each of them. Then the time constants of the CORA temperature transient are determined by least-squares fitting a model-predicted temperature corresponding to the power transient as described in [4].

This provides also a pure delay time between power and temperature transient. Then this delay time is varied in such a way that the model-predicted temperature transient fits to the initial SS-Na temperature curve. The opposite time shift of the power signal provides its precise synchronization with the CORA temperatures. This procedure also eliminates the time delay of the Cr-Al temperature signal because the response time of the SS-Na TC's is very small. The time at which the power begins to decrease is taken as the zero in the time scale for the heat balance measurements (starting point of power and temperature integrals).

V - DETERMINATION OF FUEL TEMPERATURES AND HEAT TRANSFER COEFFICIENTS FROM SA HEAT BALANCE

The heat removed from a SA during a power transient P(t) can be obtained by integrating the measured coolant temperature rise multiplied by the coolant flow rate and specific heat of sodium :

$$Q_m = hF \int_0^{\Delta t} \Delta T_m(t)\, dt \qquad (55)$$

where the integral is to be taken from the beginning of the power transient at t = 0 to several fuel time constants after the end of it at t_r :

$$\Delta t > t_r + 5\, \tau_1$$

If the final power level after the transient is not equal to zero only the transient part of the temperature rise has to be integrated ($\Delta T_m(t) - \Delta T_m(\Delta t)$).

For an ideal power step with $t_r = 0$ and constant inlet temperature this heat is given by equ. (51). However, for the real power transients this equation does not apply because their rise time is not negligible. For an AU t_r is 0,4 s but for an AR it is about 30 s.

For a real power transient the heat removed from the SA follows from equ. (50) (neglecting the last term of it) to be

$$Q = (\tau_1 + \tau_2 + Q_2)\ P^\circ + \int_o^{\Delta t} P(t)\ dt - (C_f + C_c)\,\delta T_i(\Delta t) \qquad (56)$$

which obviously is the sum of the heat removals from fuel, coolant and cladding in the fuel section and from the blanket and PNS section plus two corrections taking into account the heat generated during the transient and the increase of inlet temperature.

The heat which would be removed from the fuel only at constant inlet temperature is then equal to

$$Q_f = Q - (\tau_2 + Q_2)\ P^\circ - \int_o^{\Delta t} P(t)dt + (C_f + C_c)\ \delta T_i(\Delta t) = \tau_1\ P^\circ$$

Using equs. (4), (37′) and the identity

$$\tau_2 = \frac{\tau_c}{1-\gamma} = \frac{\gamma}{1-\gamma}\ \frac{C_c}{k} = \frac{C_c}{2hF}$$

this becomes

$$\tau_1\ P^\circ = Q - (\frac{C_c}{2} + C_a + C)\Delta T_c^\circ - \int_o^{\Delta t} P(t)\ dt + (C_f + C_c)\cdot \delta T_i(\Delta t) \qquad (57)$$

Using the measured heat Q_m and dividing by the amplitude of the SA power transient P° we obtain the fuel response time τ_1 from equ. (57).

Then the heat transfer coefficient between fuel and coolant can be calculated, either using equs. (12) and (9) :

$$k = \frac{C_f}{\tau_1 - C_f/2hF} \tag{58}$$

or using equ. (1) after having determined the fuel temperature :

$$k = \frac{P^\circ}{T_f^\circ - T_C^\circ} \tag{59}$$

For power transients ending at zero power the initial fuel temperature follows from equs. (57) and (11). However, in practice the final power level after reactor shut-down is not zero. The decay of fission products contributes to SA power. This power component is decreasing from about 5% to 3 to 2% of initial SA power in the time interval of interest here (~30s). The "residual" fission product heat (at $t \approx 30s$) is taken as a constant background power level. Its effect on the initial fuel temperature is taken into account by multiplying the temperature rise integral (55) by the total inital temperature rise divided by the amplitude of the temperature transient ($\Delta T(o)/(\Delta T(o)-\Delta T(\Delta t))$). Then the difference of the total fission product heat minus its "residual" component represents a time-dependent contribution to the SA power transient. It can be calculated from empirical relation-ships ($\sim t^{-0.1}$). The integral of SA power in equs. (56), (57) and (60) includes this compoent.

For a reactor scam (AU) from nominal operating conditions the major part of the heat removed from the SA comes from the fuel. This is due to the high temperature of the fuel and not to its heat capacity which represents only a minor part of the total SA heat capacity. Thus, the largest term in equ. (56) is $\tau_1 P^\circ$. All the others are small corrections the largest one of them being the contribution from the blanket and PNS section ($Q_2 P^\circ$) which at 90% n.p. represents about 13% of the total energy in the SA. Into adition, all parameters in equ. (57) except for the PNS heat capacity C_a can be determined with fairly good precision (< 10%) so that a good precision can be expected for the heat transfer coefficient, fuel temperature and time constant, also. This is not necessarily true for an AR-shut-down which takes about 30s. In this case the heat generated during the transient is larger than that being stored in the SA.

The heat capacities of fuel, cladding and coolant were calculated from the corresponding masses in the SA and temperature-dependent specific heat of the materials. As mentioned before, the heat capacity of the PNS cannot be determined in this way. It was obtained from the DYN calculations described in a previous paragraph. Thus, it has no influence on the intercomparison of measured and calculated fuel time constants and temperatures.

The initial SA power P° is calculated from the temperature rise ΔT° according to equ. (4) using adjusted coolant flow rates from a CORA data file (CORA.DON). This value is also used to calibrate the neutron detector signal from which the transient power integral is calculated.

In general the measured heat Q_m might be less than that given by equ. (56) due to a combined effect of fission product heat and temperature -dependent heat transfer coefficient. According to DYN calculations for the scram at 90 % n.p. the final fuel temperature of a central SA is 51 K higher than it would be according to fission product heating and constant heat transfer coefficient. The resulting error in the SA heat balance (56) would be less than - 5 %. However, in practice this effect seems to be much smaller than calculated. This can be concluded from the discrepancy between measured and calculated outlet temperature transients discussed before (Figs. 7, 8).

In the measurements the effect of a rapidly decreasing gap conductance at the beginning of the transient is missing. From the fairly good agreement of the temperature transients measured at different power levels it is concluded that the decrease of gap conductance during the transient is at least partially balanced out by the increase of fuel conductivity with decreasing temperature (Fig. 15). Thus, it is assumed that to a good approximation the heating of fuel by fission product decay is proportional to its contribution to the total SA power. Then it can be included in the heat balance in order to obtain the fuel temperature as discussed before.

Equation (57) holds exactly for constant fuel heat capacity only. However, its right-hand side is always representing the heat being stored in the fuel (Q_f) but it is not equal to

$$\tau_1 P^\circ = C_f^\circ \, (T_f^\circ - T_i^\circ) \neq Q_f$$

if the fuel heat capacity changes with fuel temperature. In this case the heat balance of the SA is given by

$$\int_{T_i^\circ}^{T_f^\circ} C_f(T)\,dT = Q_m - \left(\frac{C_c}{2} + C_a + C\right) \Delta T_c^\circ - \int_0^{\Delta t} P(t)\,dt$$

$$+ (C_f + C_c)\, \delta T_i \, (\Delta t) \qquad (60)$$

instead of equ. (57).

From Fig. 16 it can be seen that the specific heat of the fuel increases with increasing fuel temperature. As a result, the fuel heat capacity at 1700°C (43 KJ/°K) would be 24 % higher than at 400°C (34,6 KJ/°K). Its mean value

$$\bar{C}_f = \frac{1}{T_f^\circ - T_i^\circ} \int_{T_i}^{T_f^\circ} C_f \, (T) \, dT \qquad (61)$$

in the same temperature range would still differ by about 13 % from the upper and lower limits. Thus, using equ. (57) would underestimate the fuel response time τ_1 of the highest-load SA's by up to 13 %. The mean value (61) of the fuel heat capacity is changing much less with fuel temperature than the heat capacity itself :

$34,9 \leq \bar{C}_f \leq 37,5$ KJ/°K (36,2 KJ/°K ± 3,5 %)
for
$450 \leq T_f \leq 1700$°C

Therefore, fairly good estimates of the heat transfer coefficient and fuel temperature can be obtained from equs. (57) to (59) and (11) using this mean value. In this way the error in time constant is partly balanced out.

Newertheless, in order to obtain these parameters with the highest possible accuracy they were determined in a different way. The fuel temperature $T_f°$ was derived directly from the heat stored in the fuel by iteratively solving (Newton's formula) the integral equation

$$\int_{T_i}^{T_f} C_f\,(T)\,dT - Q_f = 0 \qquad (62)$$

For this purpose the empirical relationship [9]

$$\begin{aligned} C_p(T) = &- 9{,}8472.10^{2}\,(T + 273)^{-2} + 243{,}71 + 0{,}3044T \\ &- 4{,}8541.10^{-4}T^{2} + 4{,}4916.10^{-7}T^{3} - 2{,}6937.10^{-10}T^{4} \\ &+ 9{,}9528.10^{-14}T^{5} - 1{,}4325.10^{-17}T^{6}\ [J/kg\ °C] \end{aligned} \qquad (63)$$

between specific heat and temperature of fuel and the equation

$$C_f(T) = M_f\ C_p(T) = 104{,}8\ \ C_p(T) \qquad (64)$$

for the fuel heat capacity were used with an average fuel mass per SA M_f=104,8 kg which follows from fuel fabrication parameters /11/.

Then, from the fuel temperature $T_f°$ the heat capacity, the heat transfer coefficient and the time constant were calculated using equs. (64), (1) and (9), respectively.

The error limits of about ± 10 % of the results are mainly determined by parameters which could not be measured as, for instance, SA coolant flow rate (± 3 %), effective heat capacity of the upper axial neutron shield (PNS) (± 3 %), the thermocouple response time (+ 7 %) as well as the sampling time of SA outlet temperatures (± 2 %). For slow reactor shut-downs (AR) the largest

error might come from the transient SA power integral (Cf. Tab. III). The effect of inherent temperature fluctuations on measured SA temperature rise was eliminated by averaging the temperature signals during 50 s before and 10 s after the transient.

VI - RESULTS

Outlet temperature transients of SPX1 subassemblies have been analysed for six power levels between 15 and 90 % n.p.

For the transients of 34 and 50 % n.p. there is no CORA perturbography. The transients measured with KASUMOS are from four blanket and four fuel elements selected for other purposes. Three of these fuel elements are located at the core periphery (row 11) where the SA outlet temperature is influenced by recirculating pool sodium. Thus, in these two cases only one SA outlet temperature transient could be analysed (central position 2831). This SA is representative for the inner core and corresponds to the fuel channel 1 ("derivation 1") in the core model of the DYN2 code.

For the 15 % n.p. transient the neutron power could not be measured. The normalized power integral was taken from a similar measurement. Into addition, the perturbography was incomplete in this case. It provided only 279 instead of 429 outlet temperatures (237 fuel and 42 blanket SA's). The time of the scram had to be extrapolated from other measurements.

Reactor operating conditions and experimental parameters as well as measured and calculated results are summarised in Tab. III. Time constants, fuel temperatures and heat transfer coefficients are given for one central SA (2831) and the corresponding channel of DYN2 besides of core mean values with and without the last SA row.

In Figs. 17 to 19 these parameters are plotted versus reactor power. It is seen that measured fuel time constants and heat transfer coefficients are nearly constant from 34 to 90 % n.p. The variations at lower power levels might be the combined effect of decreasing fuel conductivity and increasing gap conductance with increasing SA power. It should also be pointed out that for these measurements the accuracy is less than for the measurements at high power because the correction terms in equ. (57) become more important for decreasing SA power and coolant flow rate.

Except for the results at 23 % n.p. in Figs. 17, 18, the measured curves are similar to the calculated ones although the measured time constants and fuel temperatures are higher than those obtained from the calculations with DYN2. The calculated fuel temperature curves in Fig. 18 show a decreasing gradient between 50 % and 80 % n.p. which indicates an improvement of the heat transfer between fuel and coolant. This was not found in the measurements.

Complete listings and core maps of measured individual parameters of all fuel assemblies can be obtained in the interactive evaluation of the temperature transients with KASUMOS. They are not included in this report. Only core minimum, mean and maximum values as well as standard deviations obtained thereof by a statistical analysis are given in Tab. IV to Tab. VII. Statistics parameters were determined separately for the last SA row to show the effect of coolant mixing in the upper plenum. To eliminate this effect on core averages, parameter statistics was also done without the last (11^{th}) SA row i.e. for couronnes no.1 to 10 only. Core maps of measured SA parameters are given for 90% of nominal reactor power only.

The effect of coolant mixing was found earlier in outlet temperatures of fuel and blanket SA's at the core-blanket boundary /10/. Coolant mixing increased the outlet temperature fluctuations in this core region as well as the mean outlet temperature of the breeder elements. In Fig.20 the standard deviation of all outlet temperatures at 90% n.p. are shown in a core map to illustrate this effect.

The heat balance after reactor shut-down from any initial power level always showed that the peripheral fuel elements with an increased outlet temperature noise level also give a higher than average SA time constant which is equal to the difference between normalized temperature rise and neutron power integrals over the transient. This is shown in Fig. 21 for the reactor scram at 90% n.p. Obviously, incresaed temperature noise and time constants are correlated at peripheral fuel SA's. Therefore, they are separately averaged.

In Figs. 22 to 27 core maps with SA coolant flow rates and power, coolant temperature rise as well as fuel time constants, fuel temperatures and heat transfer coefficients at 90% of nominal reactor power are presented.

The large number of fuel assemblies with different operational parameters in the SYX1 core provides the possibility to determine SA fuel temperatures and heat transfer coefficients as a function of SA power (or other parameters) from a single reactor scram. This can be done with fairly good accuracy by averaging the parameter of interest over the subassemblies with about the same power, for instance.

This was done for the reactor scrams from 15, 23, 80 and 90% of nominal power only. In these cases CORA "perturbographies" with SA outlet temperature transients were available. At 34 and 50% n.p. the outlet temperature of only one fuel assembly (core position 2831) could be recorded. The power range between minimum and maximum SA power was divided into 20 intervals of same width (power classes). Then both the SA power and the corresponding parameter of interest were averaged in each class. The resulting set of related mean values is representing the SA parameter as a function of SA power.

The available experimental data cover the range of SA power between about one and ten MW. In Fig. 28 the mean fuel temperature in a SA as a function of SA power obtained in this way is shown. Obviously, in the SPX1 fuel elements the mean fuel temperature increases linearly with SA power. This indicates that at least for low burn-up (up to 6000 MWd/t) the thermal resistance between fuel and coolant does not change significantly with power. This is confirmed by Fig.29 wherein the over-all heat transfer coefficient between fuel and coolant within a SA as well as SA and fuel time constants are plotted versus SA power.

A possible explanation of this phenomenon might be that the increase in fuel pin gap conductivity is balanced - out by the decrease of thermal conductivity of the fuel when the fuel temperature increases with power (cf. Fig.15).

A statistical analysis of measured SA parameters providing probability density functions was also performed. As an example in Fig. 30 this function is shown for the fuel time constant and the heat transfer coefficient at 15% and 90% of n.p. As

could be expected from the statistical parameters given in Tab.IV to Tab, VII these curves represent quite narrow non-Gaussian distributions. Except for 23% n.p. the shape of these functions did not change significantly with reactor power.

VII - CONCLUSIONS

The experimental results obtained at SPX1 showed that mean SA fuel temperatures and heat transfer coefficients between fuel and coolant can be measured with fairly good accuracy by a simple heat balance during fast reactor shut-down. This method requires neither special instrumentation nor additional data aquisition systems at SPX1. However, for future measurements at full power and higher fuel burn-up a neutron power signal should be included in CORA fast perturbographies (instead of the mean coolant inlet temperature). This would facilitate monitoring of fuel performance with increasing burn-up.

In the presented measurements up to 83 EFPD fuel burn-up and 90% of nominal power no significant change of heat transfer parameters was found. Furthermore, there was no important difference in fuel time constants and heat transfer coefficients of individual subassemblies in spite of the fact that there are significant differences in SA power and fuel burn-up of SA's at different core positions (about a factor of 1.5).

However, measured fuel temperatures were in all cases clearly higher than those calculated with the SPX1 system's code DYN2. The difference between measured and calculated core mean values of fuel temperature increases from 50 K at low power to 181 K at 90% nominal power. This could be due to an overestimation of the heat transfer coefficient by about 20% in the calculations. Discrepancies were also found in transient heat transfer at high power levels. From the different shape of measured and calculated SA outlet temperature transients it might be concluded that the change of heat transfer in the fuel-clad interspace during the transient is not exactly reproduced in the computer code.

The measurements provide a two-dimensional fuel temperature profile of the core which is not obtained from the calculations. This could be used for calculating space-dependent reactivity feedback effects depending on fuel temperature.

ACKNOWLEDGEMENT

This work was performed within the framework of French-German cooperation in the field of fast breeder reactor development. The measurements at SPX1 and most of the analysis were performed during the authors stay at C.E.A./C.E.N. Cadarache, France. The continuous support and assistance of persons from various services of the Département des Réacteurs à Neutrons Rapides (D.R.N.R.) is greatly acknowledged.

REFERENCES

[1] M. EDELMANN et al.
Intercomparison of noise analysis and perturbation techniques for measuring fast reactor fuel element performance characteristics.
Proc. SMORN IV, Prog. Nucl. En., Vol. 15 (1985), 43.

[2] M. EDELMANN, J.P. GIRARD, H. MASSIER
Experimental investigations of correlations between neutron power and fuel element outlet temperatures of SUPER PHENIX 1.
SMORN V : 5th Internat. Conf. on reactor noise.
MUNICH, October 12-16, 1987. In: Prog. Nucl. En., Vol. 21 (1988), 367

[3] R. WEBSTER
A power perturbation technique for the measurement of fuel-to-coolant heat transfer coefficients in fast reactors.
Nucl. Eng. & Design. 62 (1980), 241.

[4] M. EDELMANN, B. BERTHET, C. ESSIG, M. VANIER
Measurement of the fuel-to-coolant heat transfer coefficient of SUPER PHENIX 1 fuel elements.
Proc. ANS/ENS Intntl. Conf. on fast breeder systems.
Sept. 13-17, 1987, Kennewick, U.S.A. (1987), 8.13-1

[5] J. GOURDON, A. JEANNOT
Evolution du système de surveillance et de protection du coeur des réacteurs rapides.
Proc. of IAEA Sympos. Nucl. power plant control and instrument., CANNES (April 24-28,1978), Vol. II, 23.

[6] M. EDELMANN, H. MASSIER
Functions and structure of the Karlsruhe subassembly monitoring system KASUMOS.
Proc. SMORN III, Prog. Nucl. En., Vol. 9 (1982), 389.

[7] M. EDELMANN
Simulation of fuel element thermal hydraulics for sensitive monitoring of coolant flow.
Proc. IAEA/NPPCI Spec. Meet. Munich (1979), Report GRS-19, Ges. f. Reaktorsicherheit, Koeln, 455

[8] J. GOURDON, R. CASEJUANE
Off-line and on-line noise analysis for core surveillance of French LMFBR - ANABEL.
Proc. SMORN III, Prog. Nucl. En., Vol. 9 (1982), 365.

[9] P. ANZIEU
C.E.N. Cadarache, unpublished report.

[10] D. LETEINTURIER et al.
C.E.N. Cadarache, unpublished report.

[11] J. HOMMET, D. LAFOND, T. NEWTON, J.Y. PIPAUD
C.E.N. Cadarache, unpublished report.

TABLE I

SA MODEL PARAMETERS OF SPX1

Symbol	Parameter	Equ.	Typical values at 15 %	Typical values 90 % n.p.	Dimensions
C_f	Fuel heat capacity	-	35,9	39,5	KJ/K
C_c	Coolant heat capacity (1)	-	34,6	34,6	KJ/K
k	Heat transfer coefficient (2)	-	7,8	7,8	KW/K
F	Coolant flow rate	-	15,0	41,2	Kg/s
γ	Feedback parameter	(6)	0,17	0,072	1
τ_f	Fuel time constant	(9)	4,6	5,1	s
τ_c	Coolant time constant	(25)	0,75	0,31	s
a	Transfer function parameters	(26)	1,5	3,4	s^{-1}
b		(27)	0,24	0,59	s^{-2}
τ_1	Fuel response time	(29),(30) (33)	5,49 5,54	5,45 5,50	s s
τ_2	Coolant response time	(29),(31) (34)	0,76 0,63	0,31 0,29	s s
τ	SA response time (2)		8,4	5,9	s

(1) including fuel pin clad.

(2) measured mean values.

TABLE II

EQUIVALENT MODEL PARAMETERS AND FUNCTIONS FOR FUEL AND PNS SECTIONS OF THE SPX1 SA

Fuel section			Blanket + PNS	
Parameter	Symbol	Equ.	Symbol	Parameter
Fuel heat capacity	C_f	-	C_a	Blanket + PNS heat capacity
Coolant heat capacity	C_c	-	C	Coolant heat capacity
Heat transfer coefficient	k	-	k_a	
Transfer function	H(s)	(23),(28) (32)	G(s)	
Fuel time constant	τ_f	(9)	τ_a	PNS time constant
Coolant time constant	τ_c	(25)	τ	PNS coolant time constant
Feedback parameter	γ	(6)	γ_a	PNS feedback parameter
Transfer function parameters	a	(26)	A	
	b	(27)	B	
Fuel response time	τ_1	(30),(33)	τ_3	PNS response time

TABLE II (continued)

Fuel section			Blanket + PNS	
Parameter	Symbol	Equ.	Symbol	Parameter
Coolant response time	τ_2	(31),(34)	τ_4	PNS coolant response time
Coefficient	Q_1	(37)	Q_2	
Coolant inlet temperature	$T_i(s)$	(38)	$\Delta N(s)$	
Initial inlet temperature	T_i°	-	1	
Transient inlet temperature	$\delta T_i(s)$	(35)	$\Delta N(s) - \frac{1}{s}$	
SA power	$P(s)$		0	
Temperature rise	$\Delta T_c(s)$	(8)	$\delta\Delta T(s)$	
Initial temperature rise	ΔT_c°	-	0	
Mean coolant temperature	$T_c(s)$	-	-	
Coolant outlet temperature	$T_o(s)$	-	-	

Consistent use of functions and parameters of this table in the model equations provides either fuel or PNS results (except normalized coolant temperatures - equs. (38) to (46) - which do not apply to the PNS section).

TABLE III

EXPERIMENTAL CONDITIONS AND RESULTS

Power level	15	23	34	50	80	90	[% n.p.]
Date	4.6.86	17.2.86	16.6.86	19.7.86	2.12.86	26.5.87	
Type of transient	AU	AR	AR	AU	AU	AU	
Primary pump speed	160	235	265	325	425	425	r /m
Primary coolant flow rate	5600	8705	9816	11661	15444	15444	Kg/s
Core inlet temperature	364	366	384	389	387	388	°C
Reactor power	508	685	1027	1546	2430	2707	MW
Core temperature rise	79	71	99	116	128	148	K
Fuel burn-up	8,8	3,6	13	20	46	83	EFPD
Time of scram in PTBR	#54	#55-0,3	-	-	#54+0,4	#54+0,4	-
Transient power integral	0,3	8,7	9,15	0,41	0,39	0,34	-
Eff. PNS heat capacity	44,5	48,4	44,5	44,5	44,5	44,5	KJ/K
Measured SA time constant position 2831	8,24	7,38	6,43	6,14	5,88	6,11	s
Calculated SA time constant derivation 1	-	5,99	6,02	5,71	4,97	5,23	s

TABLE III (continued)

Power level	15	23	34	50	80	90	[% n.p.]
Measured mean SA time const	8,37	6,98	-	-	5,90	5,90	s
Measd. fuel time const. pos. 2831	4,37	4,93	4,31	4,35	4,72	5,21	s
Measd. fuel time const. mean value	4,28	4,37	-	-	4,65	4,77	s
Measured fuel temperature pos. 2831	611	723	896	1057	1390	1606	°C
Measd. fuel temperature core mean value	588	665	-	-	1301	1431	°C
Calculated fuel temperature derivation 1	-	-	-	968	1211	1378	°C
Calculated fuel temperature core mean value	-	615	743	906	1126	1250	°C
Measured heat transfer coefficient pos. 2831	7,67	6,86	7,91	7,90	7,59	7,35	KW/K
Measd. heat transfer coeff., core average	7,85	7,76	-	-	7,69	7,78	KW/K

TABLE IV

SUMMARY OF EXPERIMENTAL RESULTS AT 15 % n.p., 9 EFPD

	ΔT_c°	ΔT_f°	τ_f	τ	ΔT_{cr}
	SA ROWS 1 - 10				
Minimum	69.16	140.81	3.72	7.73	2.70
Mean value	82.59	198.58	4.28	8.38	4.39
Maximum	92.57	239.65	4.87	9.20	6.53
Sigma	5.45	18.64	.23	.30	.77
	SA ROW 11				
Minimum	49.76	101.15	3.79	8.88	3.08
Mean value	64.46	124.00	4.39	9.72	5.04
Maximum	75.34	175.77	5.30	10.87	7.78
Sigma	6.19	15.37	.38	.52	1.19
	WHOLE CORE				
Minimum	49.76	101.15	3.72	7.73	2.70
Mean value	79.09	184.18	4.30	8.63	4.51
Maximum	92.57	239.65	5.30	10.87	7.78
Sigma	9.09	34.54	.27	.64	.91
	[°K]	[°K]	[s]	[s]	[°K]

	P°	T_f°	T_o	K	F
	SA ROWS 1 - 10				
Minimum	1168.97	543.55	433.26	6.87	12.39
Mean value	1555.99	603.98	446.69	7.85	14.93
Maximum	1831.39	646.37	456.68	8.95	15.77
Sigma	148.85	20.56	5.45	.41	.72
	SA ROW 11				
Minimum	691.42	491.08	413.86	6.26	10.99
Mean value	941.39	520.34	428.56	7.60	11.57
Maximum	1204.12	572.00	439.45	8.72	14.88
Sigma	125.37	17.01	6.19	.63	.87
	WHOLE CORE				
Minimum	691.42	491.08	413.86	6.26	10.99
Mean value	1437.26	587.82	443.19	7.80	14.28
Maximum	1831.39	646.37	456.68	8.95	15.77
Sigma	282.47	38.57	9.09	.47	1.53
	[MW]	[°C]	[°C]	[KW/K]	[Kg/s]

TABLE V

SUMMARY OF EXPERIMENTAL RESULTS AT 23 % n.p., 4 EFPD

	ΔT_c^*	ΔT_f^*	τ_f	τ	ΔT_{cr}
	SA ROWS 1 - 10				
Minimum	59.35	173.55	3.26	6.21	.32
Mean value	74.05	280.74	4.37	6.98	3.48
Maximum	82.96	353.97	5.20	7.79	6.31
Sigma	4.58	30.42	.32	.32	1.18
	SA ROW 11				
Minimum	45.11	122.16	3.14	6.52	.20
Mean value	60.00	190.78	4.71	8.06	4.21
Maximum	71.64	291.48	6.18	9.59	9.41
Sigma	5.54	27.03	.63	.67	1.59
	WHOLE CORE				
Minimum	45.11	122.16	3.14	6.21	.20
Mean value	71.33	263.35	4.43	7.19	3.62
Maximum	82.96	353.97	6.18	9.59	9.41
Sigma	7.32	46.36	.42	.59	1.30
	[°K]	[°K]	[s]	[s]	[°K]

	P^*	T_f^*	T_o	k	F
	SA ROWS 1 - 10				
Minimum	1623.59	576.52	425.69	6.50	19.25
Mean value	2169.14	684.09	440.38	7.76	23.23
Maximum	2552.14	759.80	449.30	10.24	25.51
Sigma	191.65	31.74	4.58	.56	1.10
	SA ROW 11				
Minimum	974.37	518.36	411.45	5.40	17.08
Mean value	1365.73	587.11	426.33	7.23	18.03
Maximum	1848.03	687.62	437.98	10.54	23.12
Sigma	187.60	27.86	5.54	.99	1.47
	WHOLE CORE				
Minimum	974.37	518.36	411.45	5.40	17.08
Mean value	2013.86	665.35	437.66	7.66	22.22
Maximum	2552.14	759.80	449.30	10.54	25.51
Sigma	370.24	49.29	7.32	.70	2.37
	[KW]	[°C]	[°C]	[KW/K]	[Kg/s]

TABLE VI

SUMMARY OF EXPERIMENTAL RESULTS AT 80 % n.p., 46 EFPD

	ΔT_c^*	ΔT_f^*	τ_f	τ	ΔT_{cr}
	SA ROWS 1 - 10				
Minimum	104.75	662.40	3.98	5.34	2.93
Mean value	132.76	899.00	4.65	5.90	5.22
Maximum	145.84	1103.59	5.51	6.60	8.84
Sigma	8.19	91.62	.28	.23	.96
	SA ROW 11				
Minimum	82.85	489.56	4.35	5.70	3.29
Mean value	108.90	646.42	5.10	6.86	6.18
Maximum	128.46	822.40	6.53	8.31	11.52
Sigma	9.99	67.05	.38	.45	1.58
	WHOLE CORE				
Minimum	82.85	489.56	3.98	5.34	2.93
Mean value	128.15	850.18	4.74	6.08	5.41
Maximum	145.84	1103.59	6.53	8.31	11.52
Sigma	12.73	132.62	.35	.47	1.17
	[°K]	[°K]	[s]	[s]	[°K]

	P^*	T_f^*	T_o	K	F
	SA ROWS 1 - 10				
Minimum	5121.28	1109.43	491.96	6.70	34.16
Mean value	6897.98	1352.59	519.97	7.69	41.21
Maximum	7959.28	1560.58	533.05	8.72	45.25
Sigma	589.50	94.58	8.19	.37	1.95
	SA ROW 11				
Minimum	3174.79	923.13	470.07	5.26	30.30
Mean value	4395.76	1088.08	496.11	6.80	31.99
Maximum	5978.13	1272.74	515.67	7.95	41.03
Sigma	583.86	70.68	9.99	.50	2.60
	WHOLE CORE				
Minimum	3174.79	923.13	470.07	5.26	30.30
Mean value	6414.36	1301.46	515.36	7.52	39.43
Maximum	7959.28	1560.58	533.05	8.72	45.25
Sigma	1149.99	138.17	12.73	.53	4.20
	[KW]	[°C]	[°C]	[KW/K]	[Kg/s]

TABLE VII

SUMMARY OF EXPERIMENTAL RESULTS AT 90 % n.p., 83 EFPD

	ΔT_c^*	ΔT_f^*	τ_f	τ	ΔT_{cr}
	SA ROWS 1 - 10				
Minimum	121.54	718.81	3.89	5.37	3.21
Mean value	153.90	1030.32	4.77	5.90	6.67
Maximum	169.06	1241.76	5.75	6.51	10.91
Sigma	9.99	108.57	.33	.20	1.22
	SA ROW 11				
Minimum	97.29	562.39	4.20	5.54	3.83
Mean value	124.82	712.11	4.94	6.70	7.54
Maximum	145.76	895.09	6.73	8.51	12.67
Sigma	10.99	64.09	.38	.45	1.74
	WHOLE CORE				
Minimum	97.29	562.39	3.89	5.37	3.21
Mean value	148.28	968.82	4.81	6.06	6.84
Maximum	169.06	1241.76	6.73	8.51	12.67
Sigma	15.35	161.53	.34	.41	1.38
	[°K]	[°K]	[s]	[s]	[°K]

	P^*	T_f^*	T_o	K	F
	SA ROWS 1 - 10				
Minimum	5963.38	1181.44	509.58	6.88	34.16
Mean value	7997.06	1495.32	541.94	7.78	41.21
Maximum	9226.85	1711.64	557.10	8.93	45.25
Sigma	705.14	112.35	9.99	.34	1.95
	SA ROW 11				
Minimum	3728.12	1003.98	485.34	5.15	30.30
Mean value	5038.50	1162.56	512.86	7.06	31.99
Maximum	6593.24	1343.19	533.81	8.32	41.03
Sigma	657.72	67.73	10.99	.52	2.60
	WHOLE CORE				
Minimum	3728.12	1003.98	485.34	5.15	30.30
Mean value	7425.24	1431.00	536.32	7.64	39.43
Maximum	9226.85	1711.64	557.10	8.93	45.25
Sigma	1359.97	168.33	15.35	.47	4.20
	[KW]	[°C]	[°C]	[KW/K]	[Kg/s]

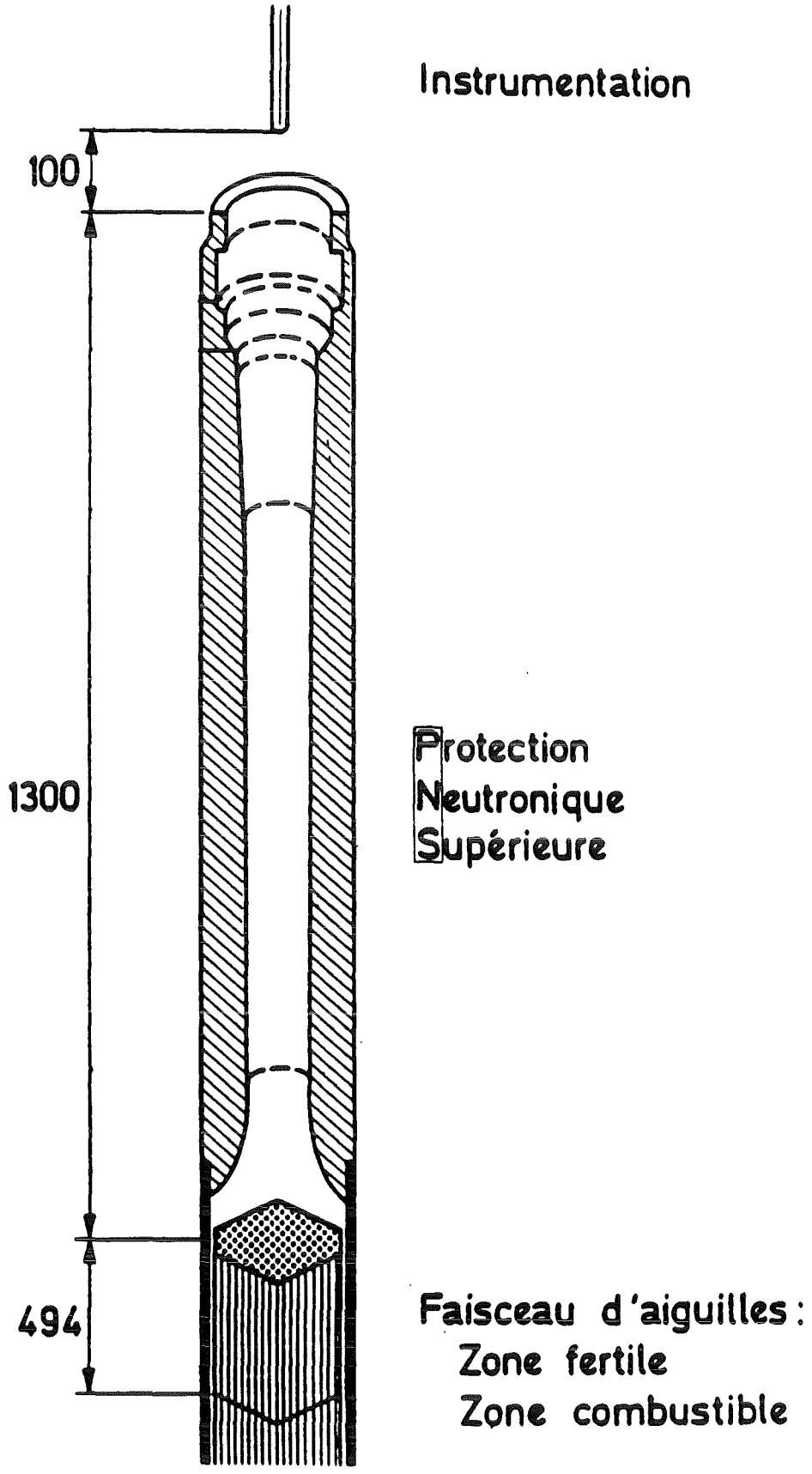

Fig. 1 SPX1 fuel element with integrated axial neutron shield (PNS)

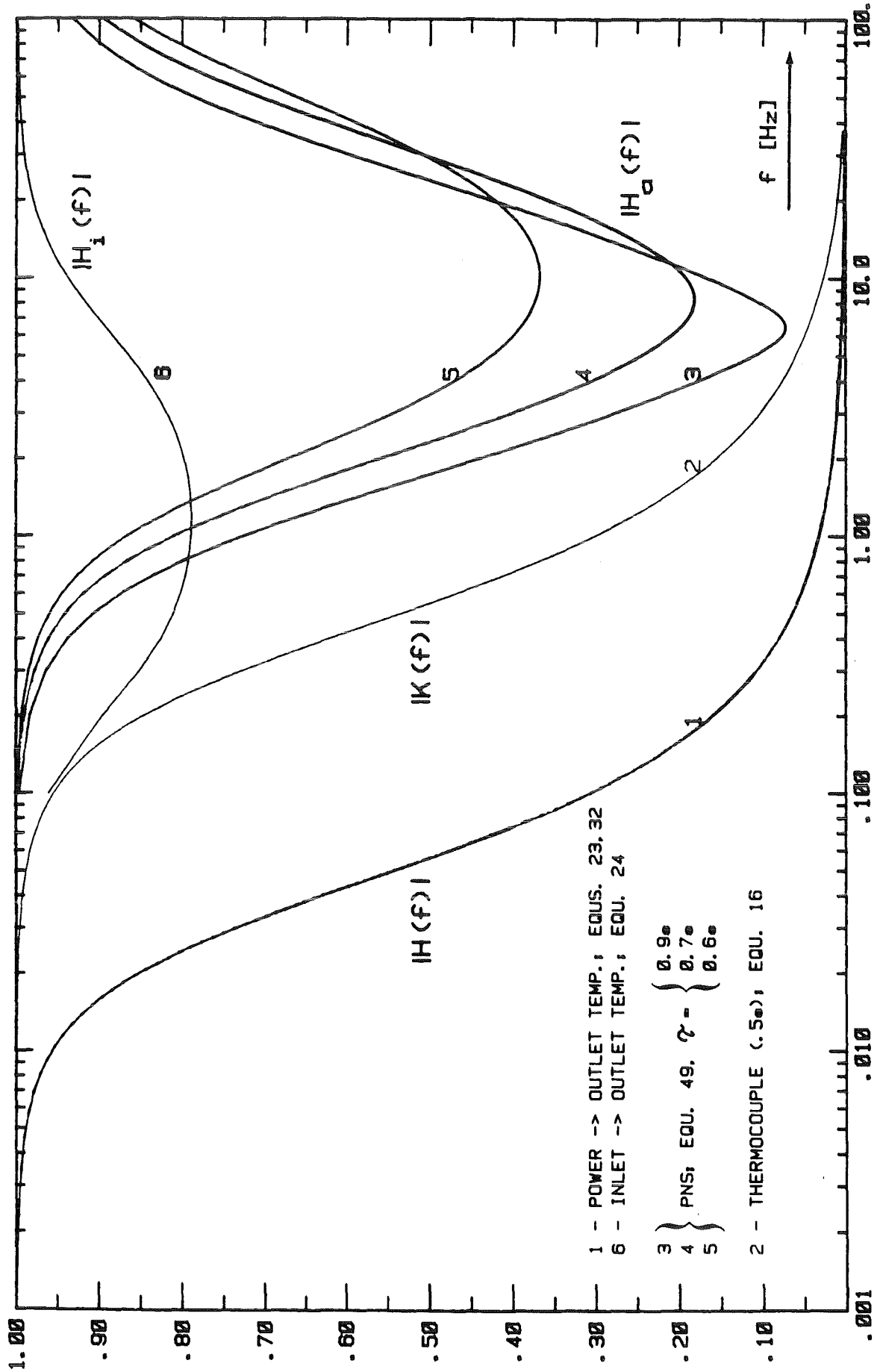

Fig. 2 Model transfer functions of fuel and PNS sections

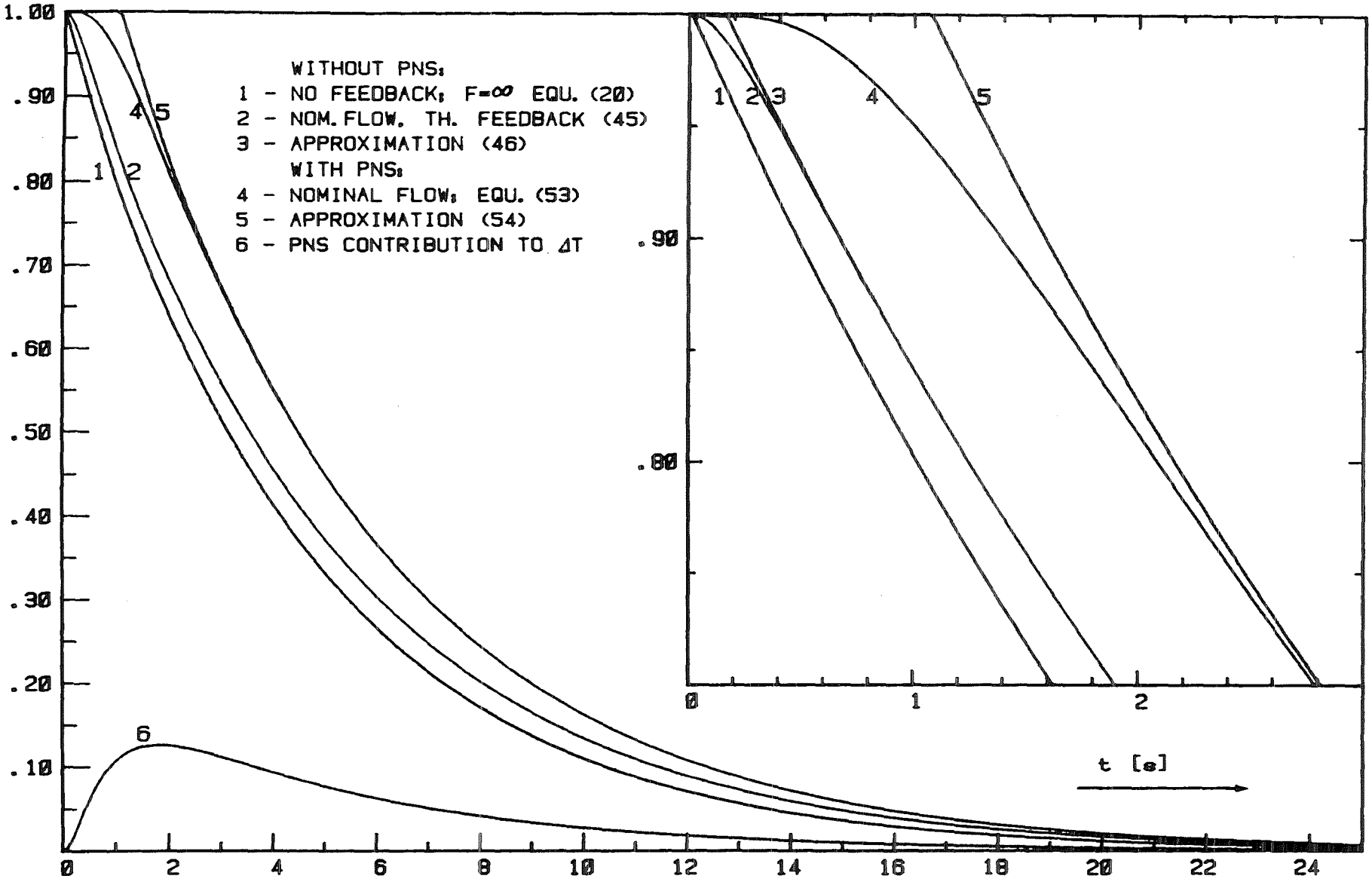

Fig. 3 Exact and approximate SA model step response functions

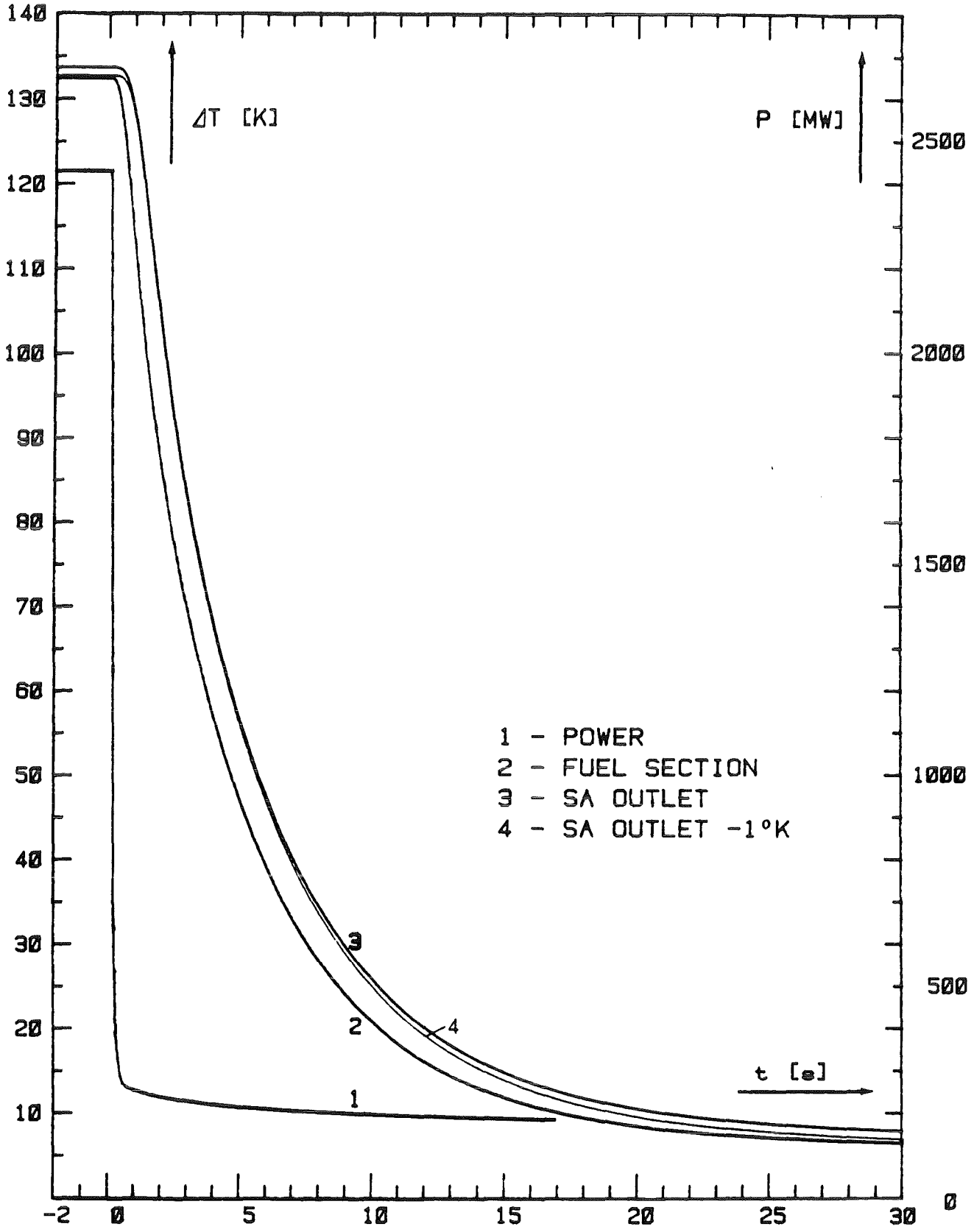

Fig. 4 DYN2-calculated power and outlet temperature transients; 80% n.p.

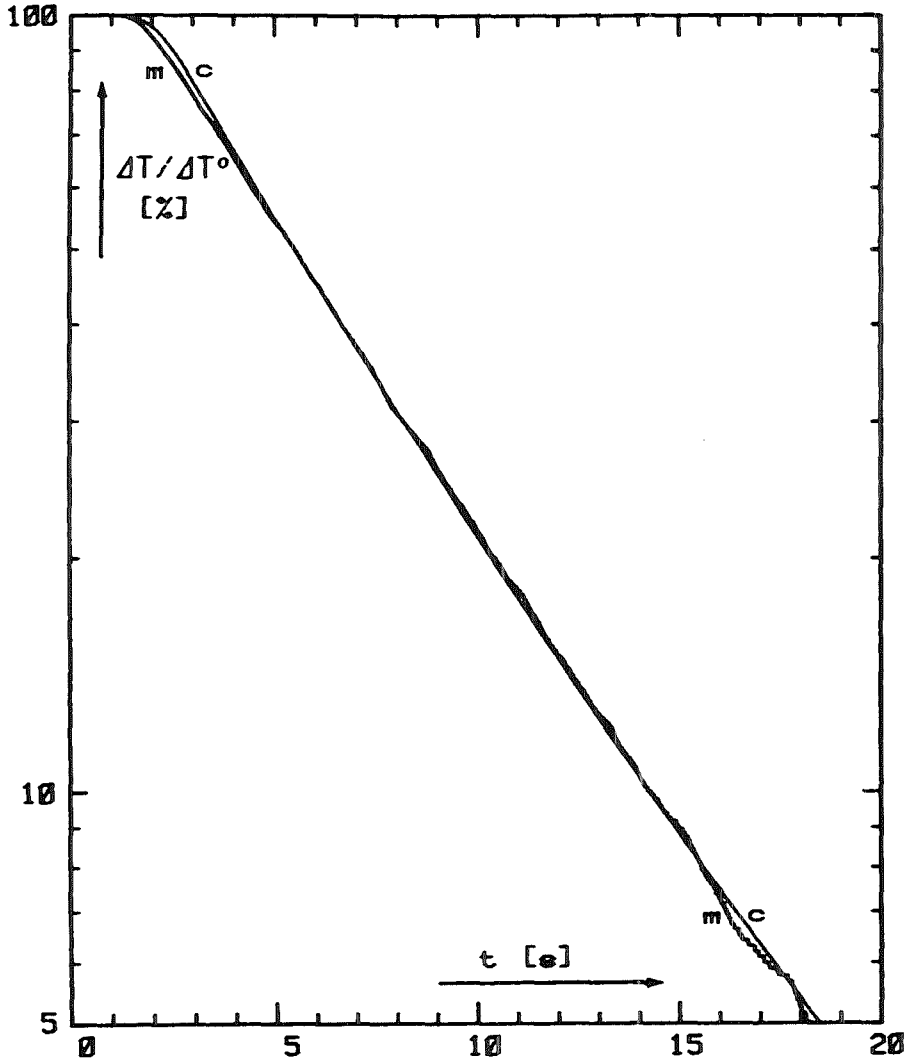

Fig. 5 Normalyzed measured and calculated (DYN2) SA outlet temperature transients; AU 50% n.p.

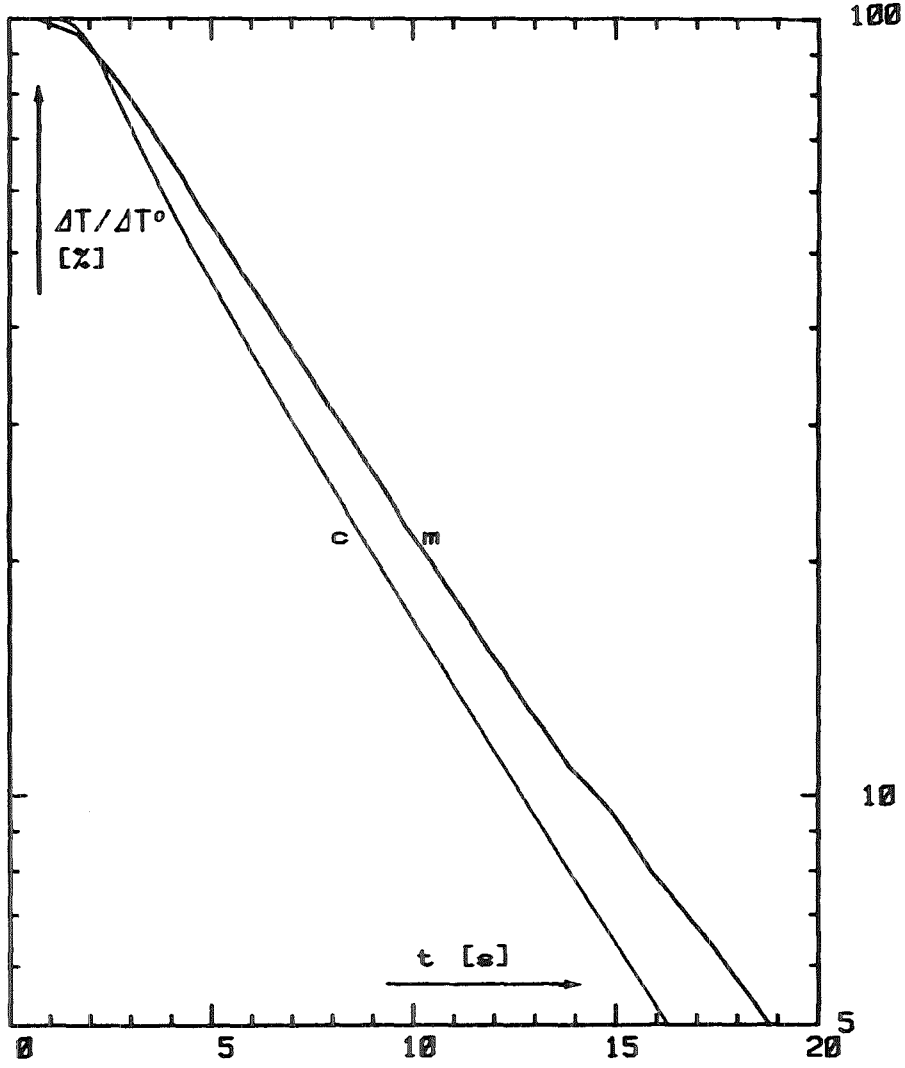

Fig. 6 Normalyzed measured and calculated (DYN2) SA outlet temperature transients; AU 80% n.p.

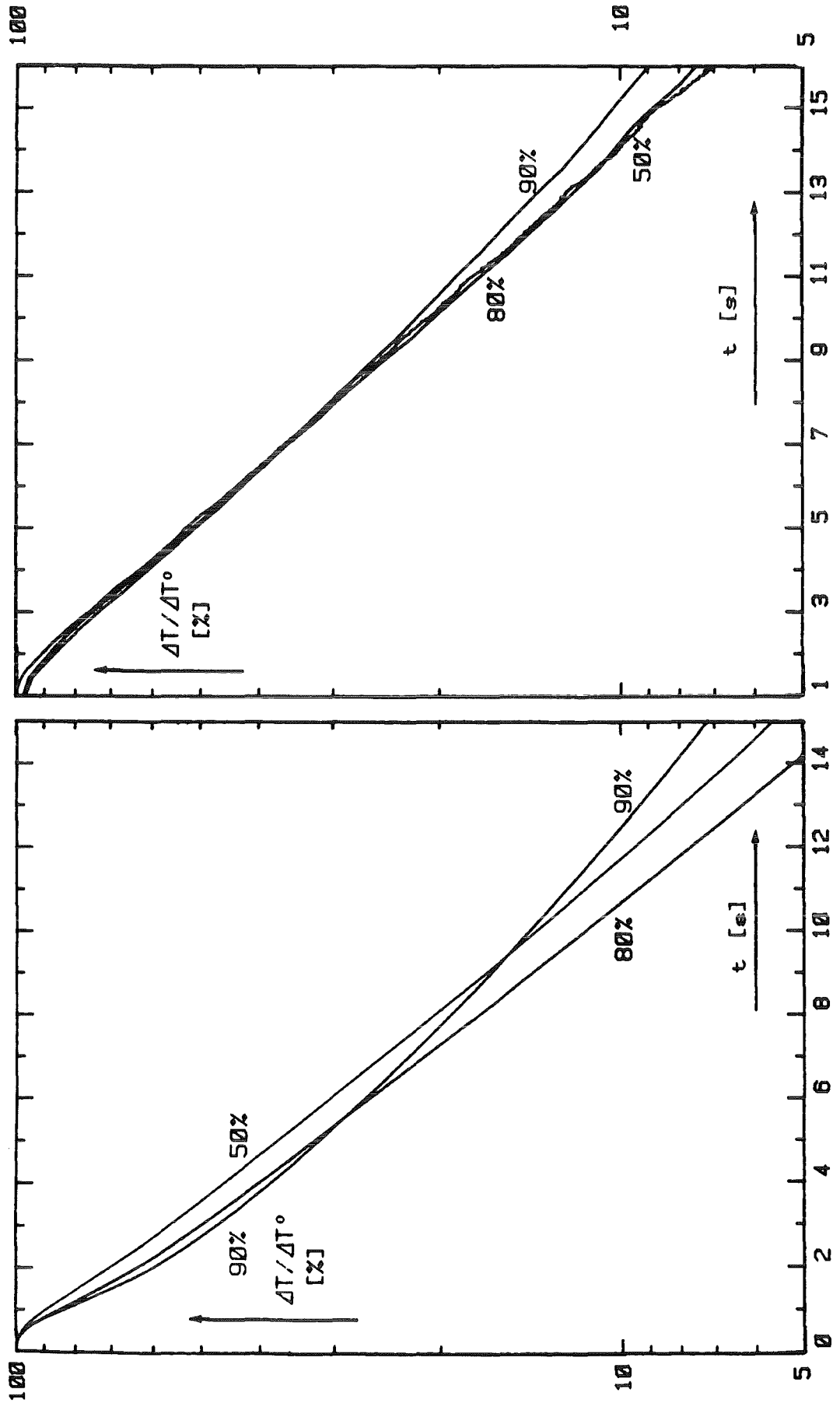

Fig. 7 DYN2-calculated SA outlet temperature transients after scram at 50, 80 and 90% n.p.

Fig. 8 Measured SA outlet temperature transients after scram at 50, 80 and 90% n.p. (normalized)

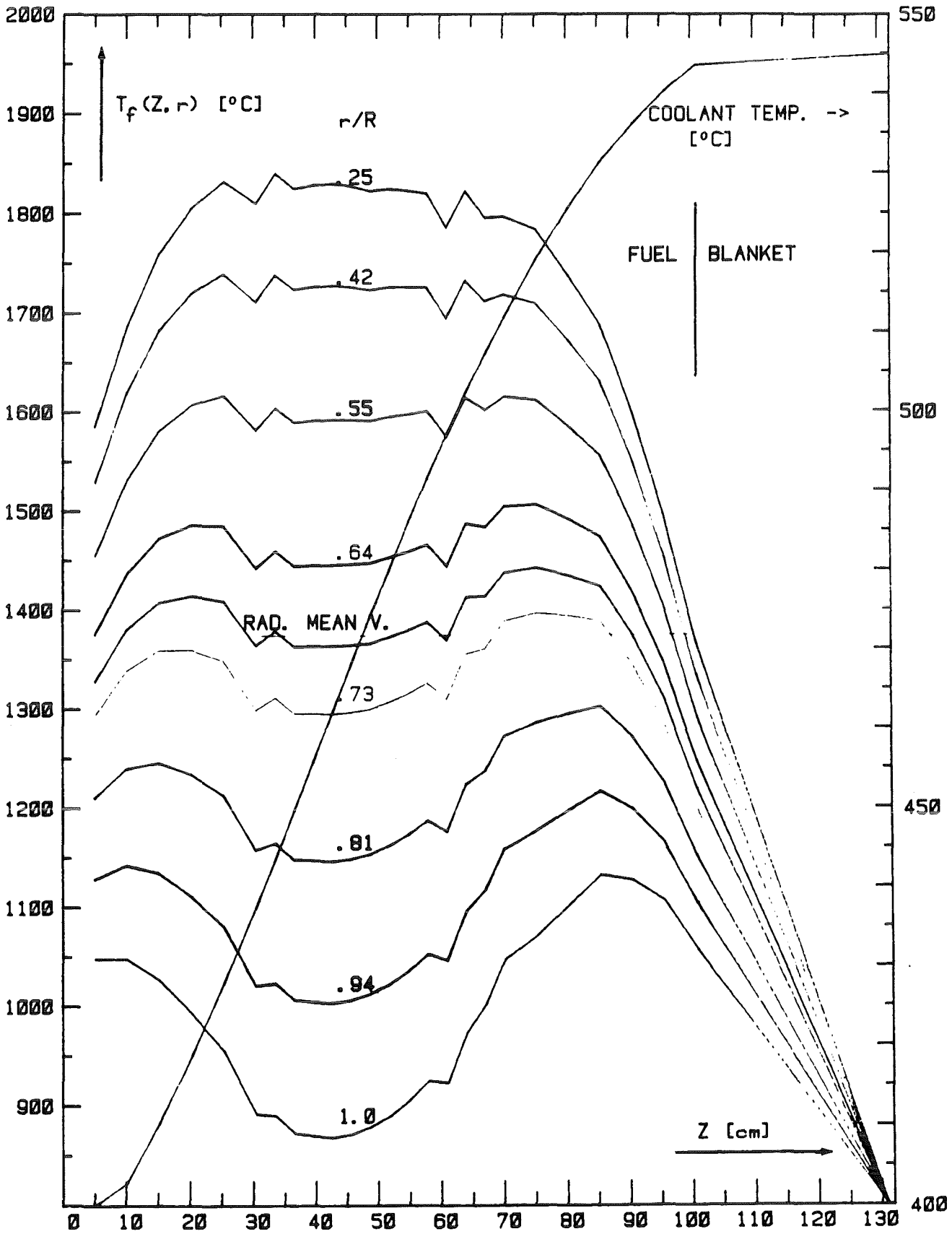

Fig. 9 Axial fuel temperature profiles at radial mesh points of DYN2; 90% n.p.

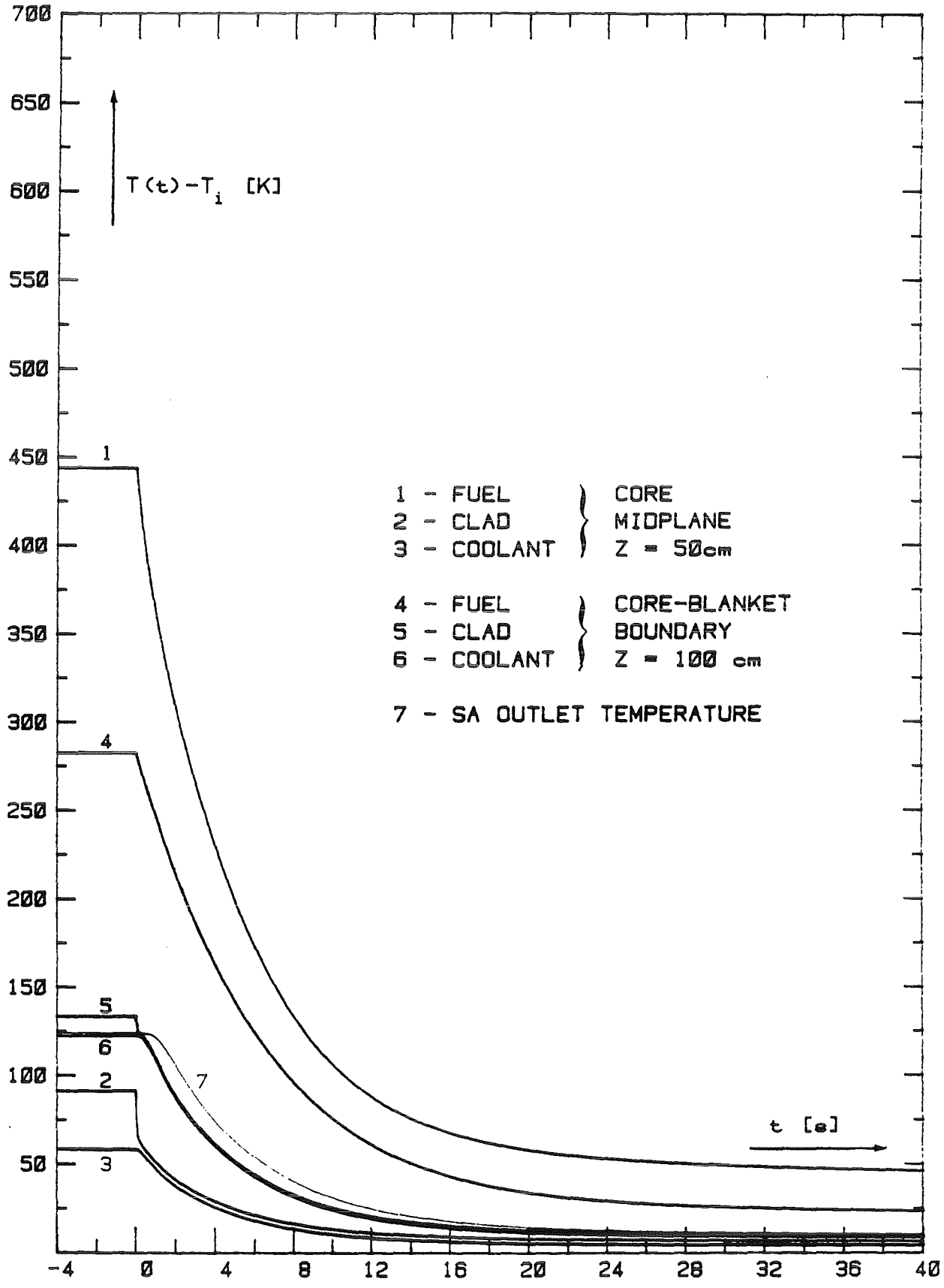

Fig. 10 Calculated fuel and coolant temperature transients; scram 50% n.p.

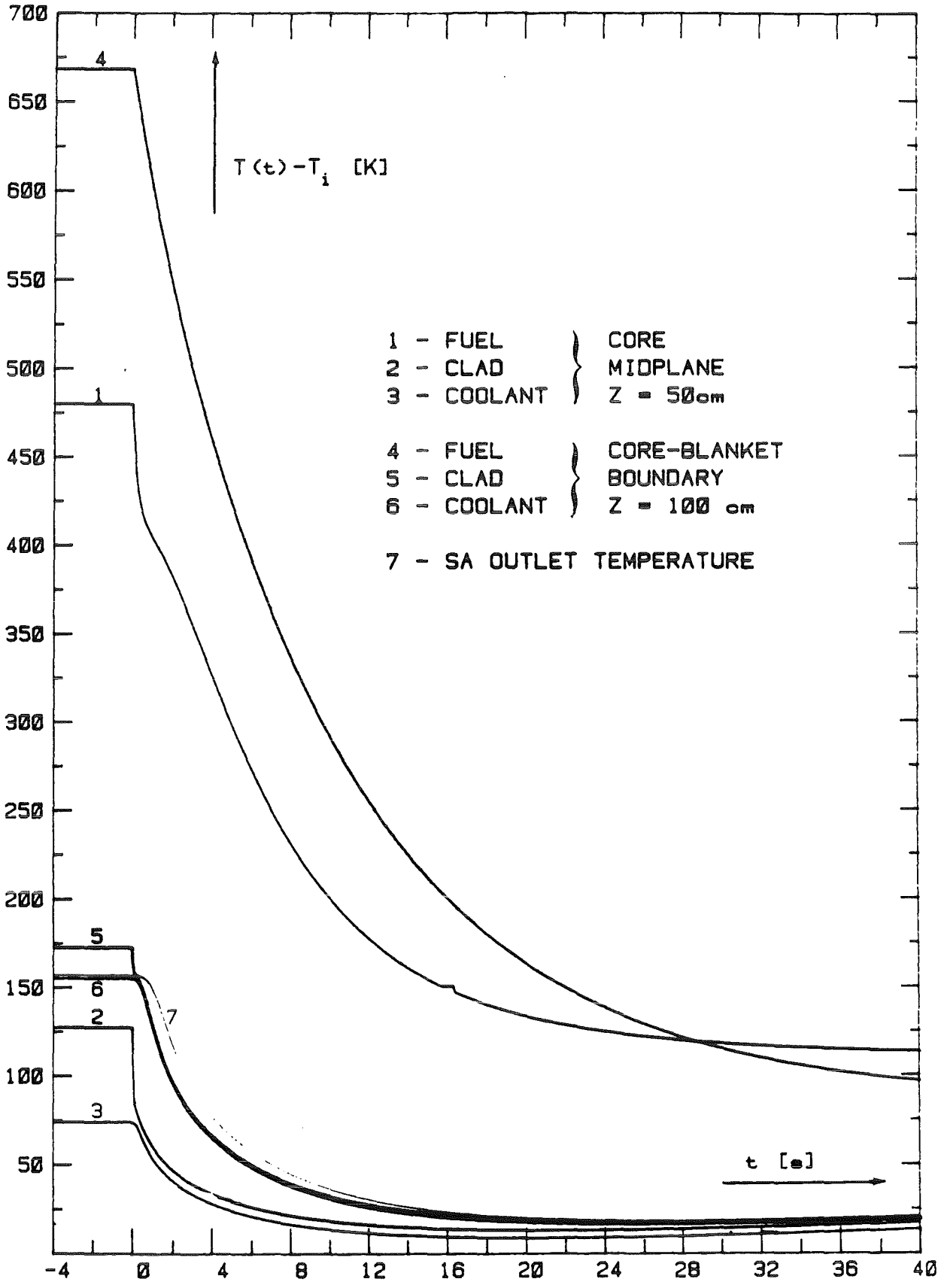

Fig. 11 Calculated fuel and coolant temperature transients; scram 90% n.p.

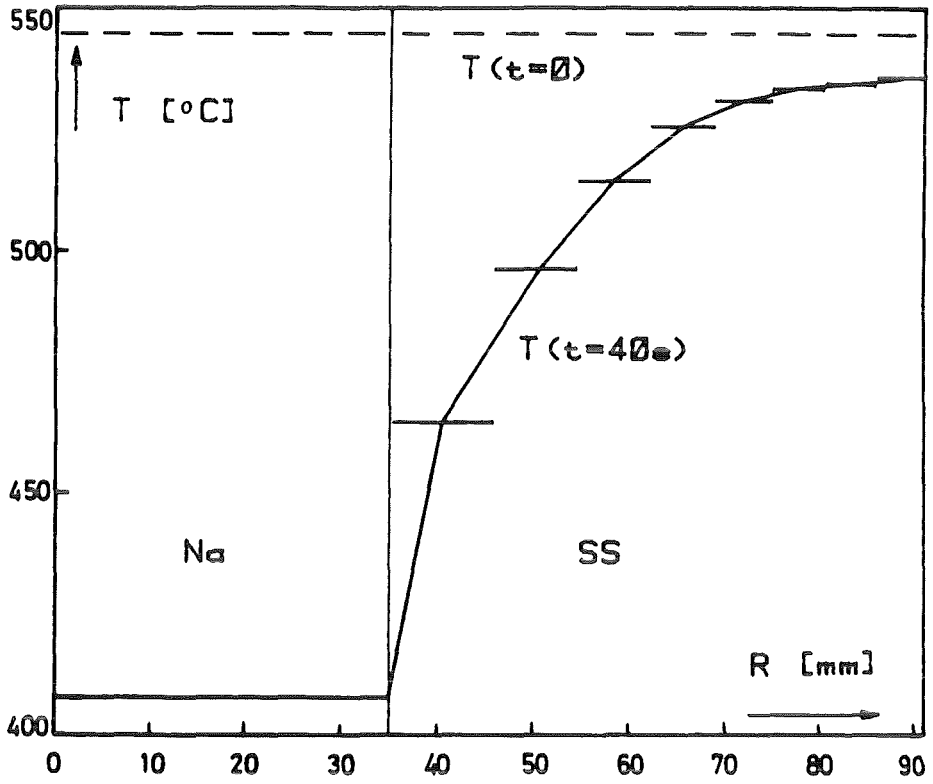

Fig. 12 Radial PNS temperature profile 40s after scram (DYN2)

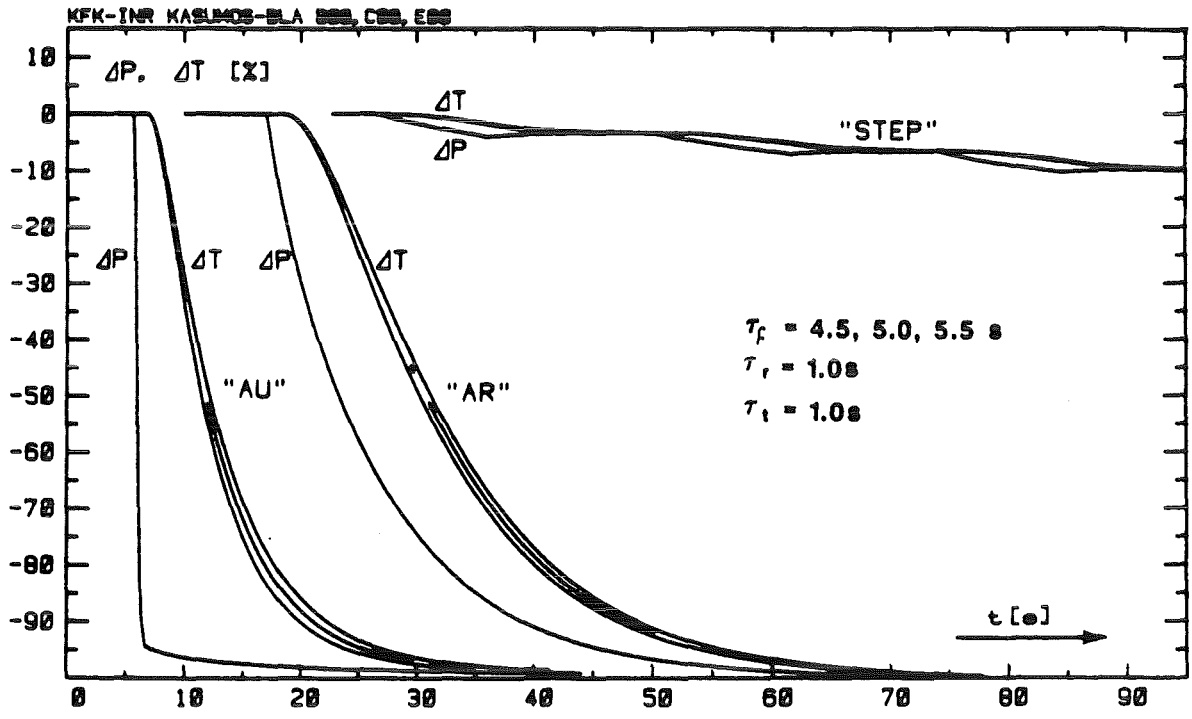

Fig. 13 Variation of outlet temperature transients with fuel time constant (+-10%) for different types of power transients

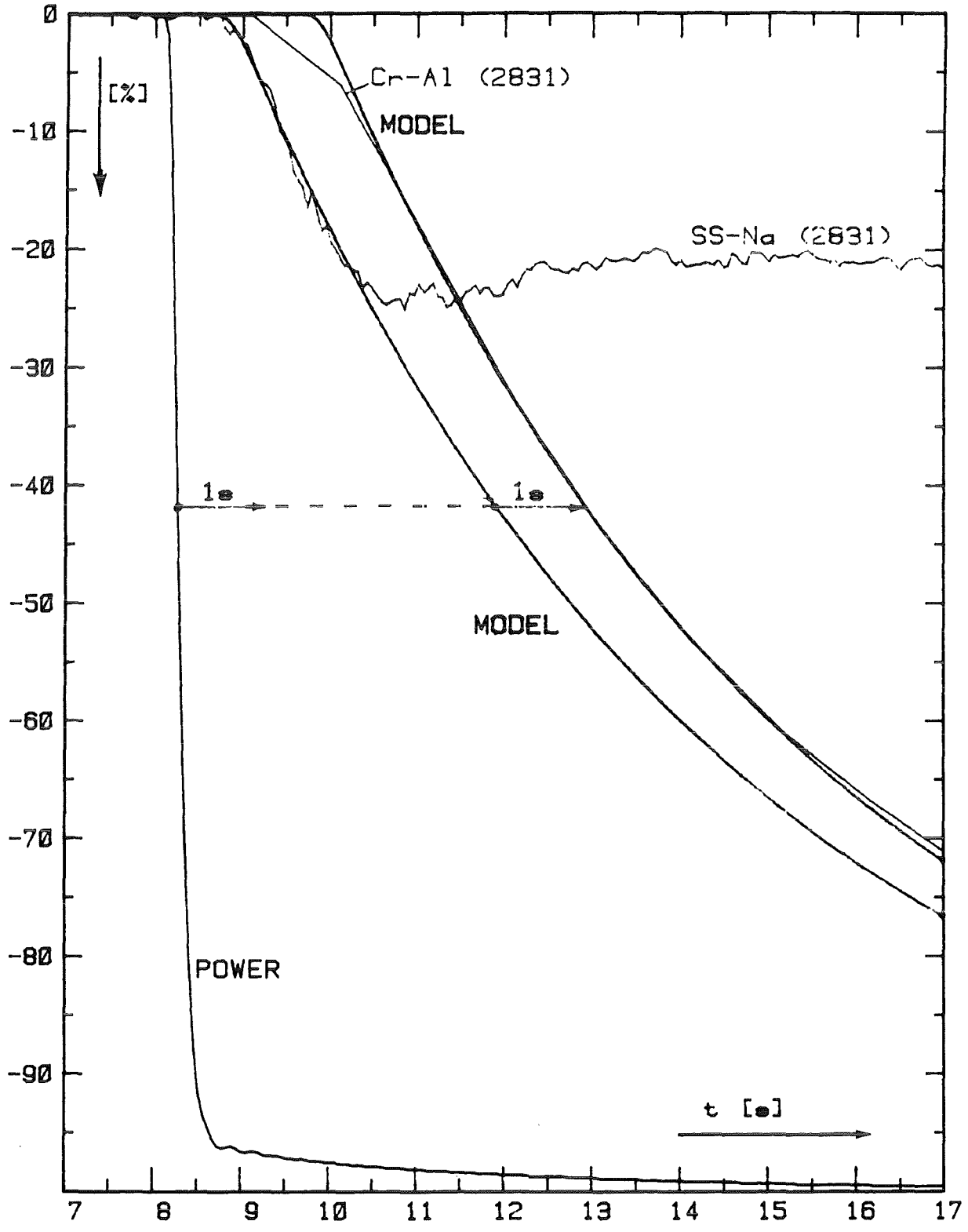

Fig. 14 Synchronization of CORA and KASUMOS perturbographies

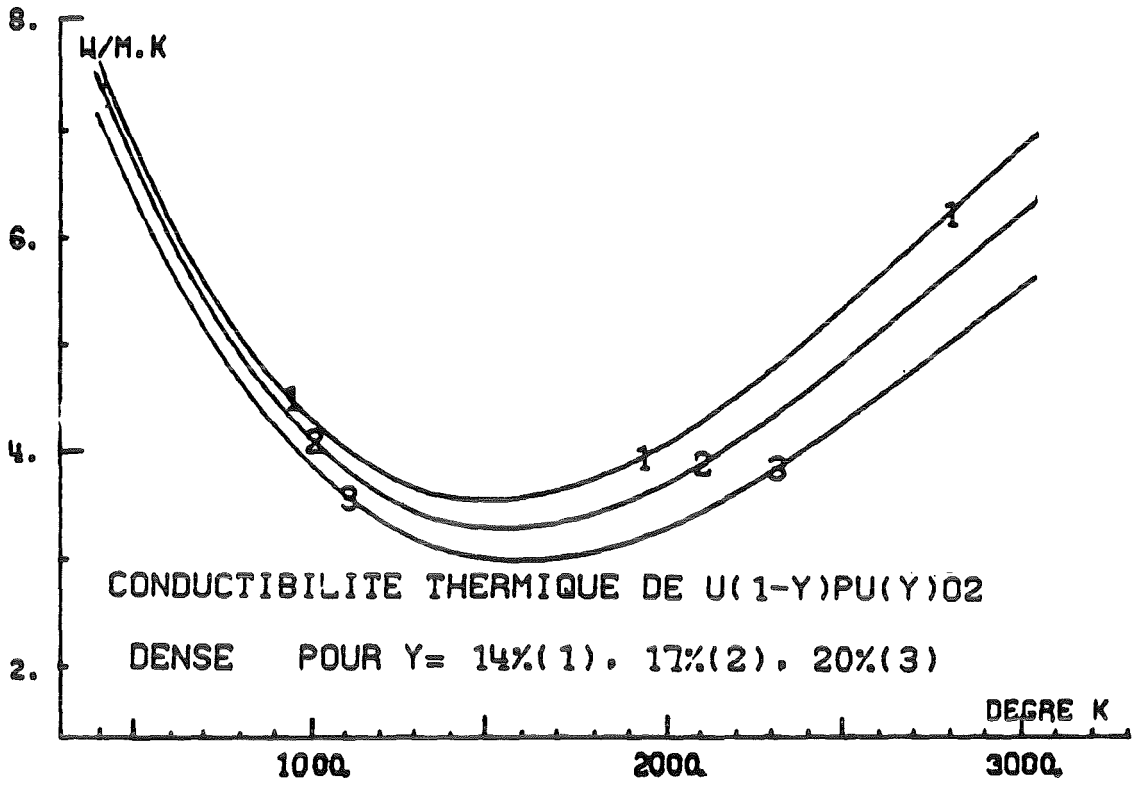

Fig. 15 Thermal conductivity of mixed oxide fuel [9]

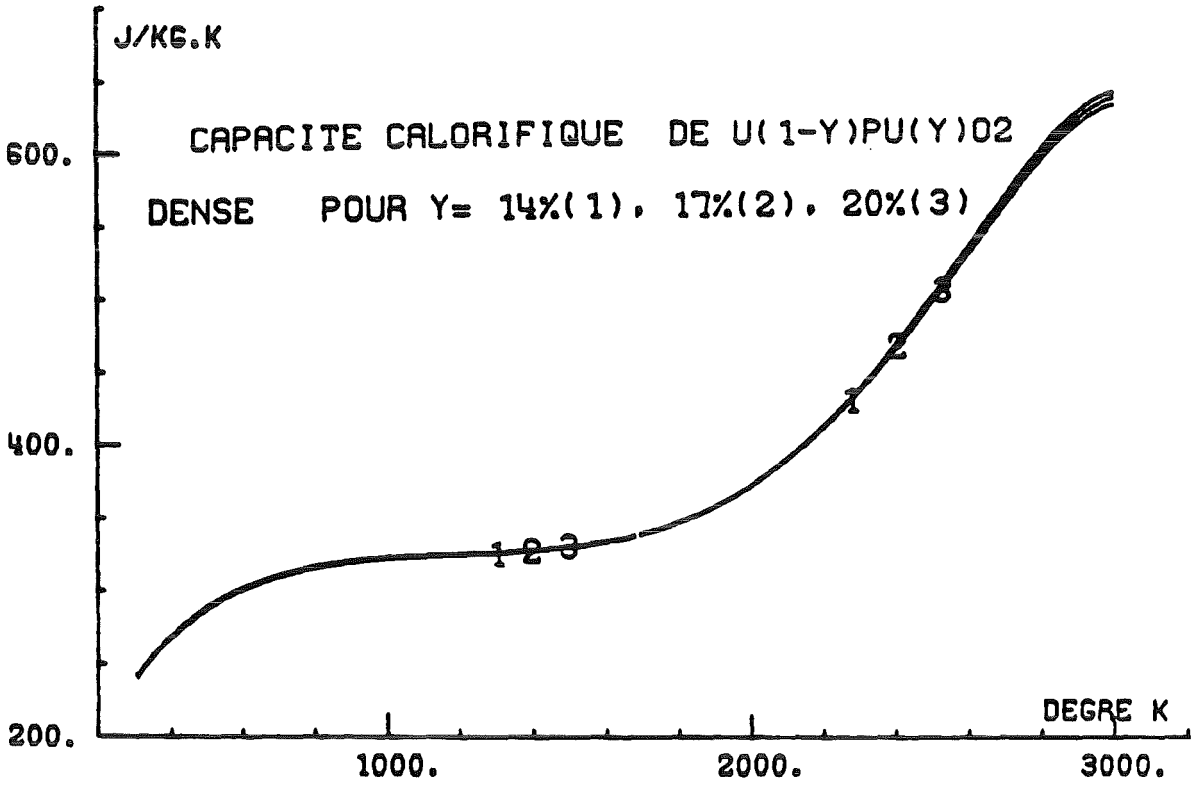

Fig. 16 Specific heat of mixed oxide fuel [9]

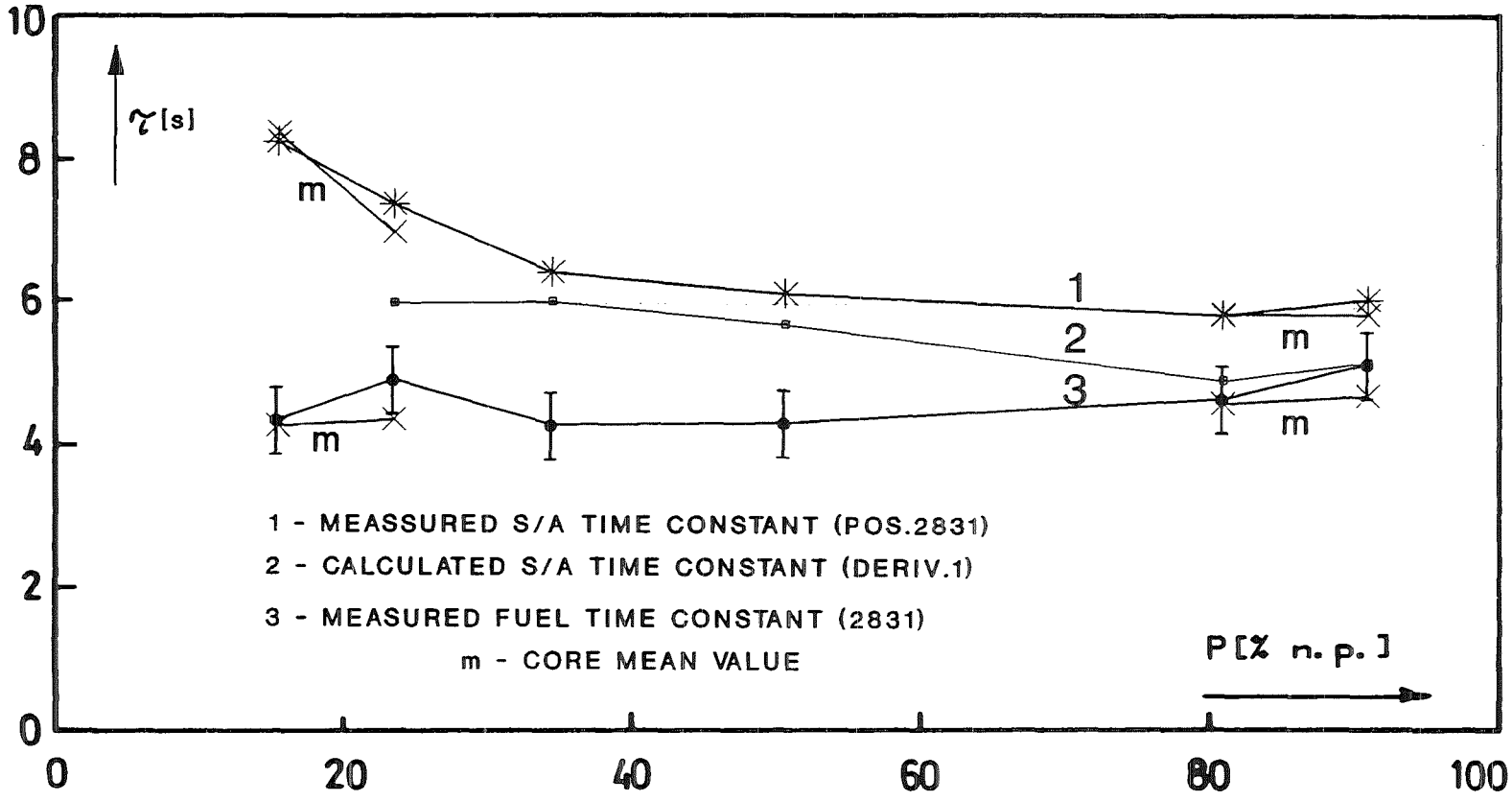

Fig. 17 Evolution of SA and fuel time constants with power and burn-up

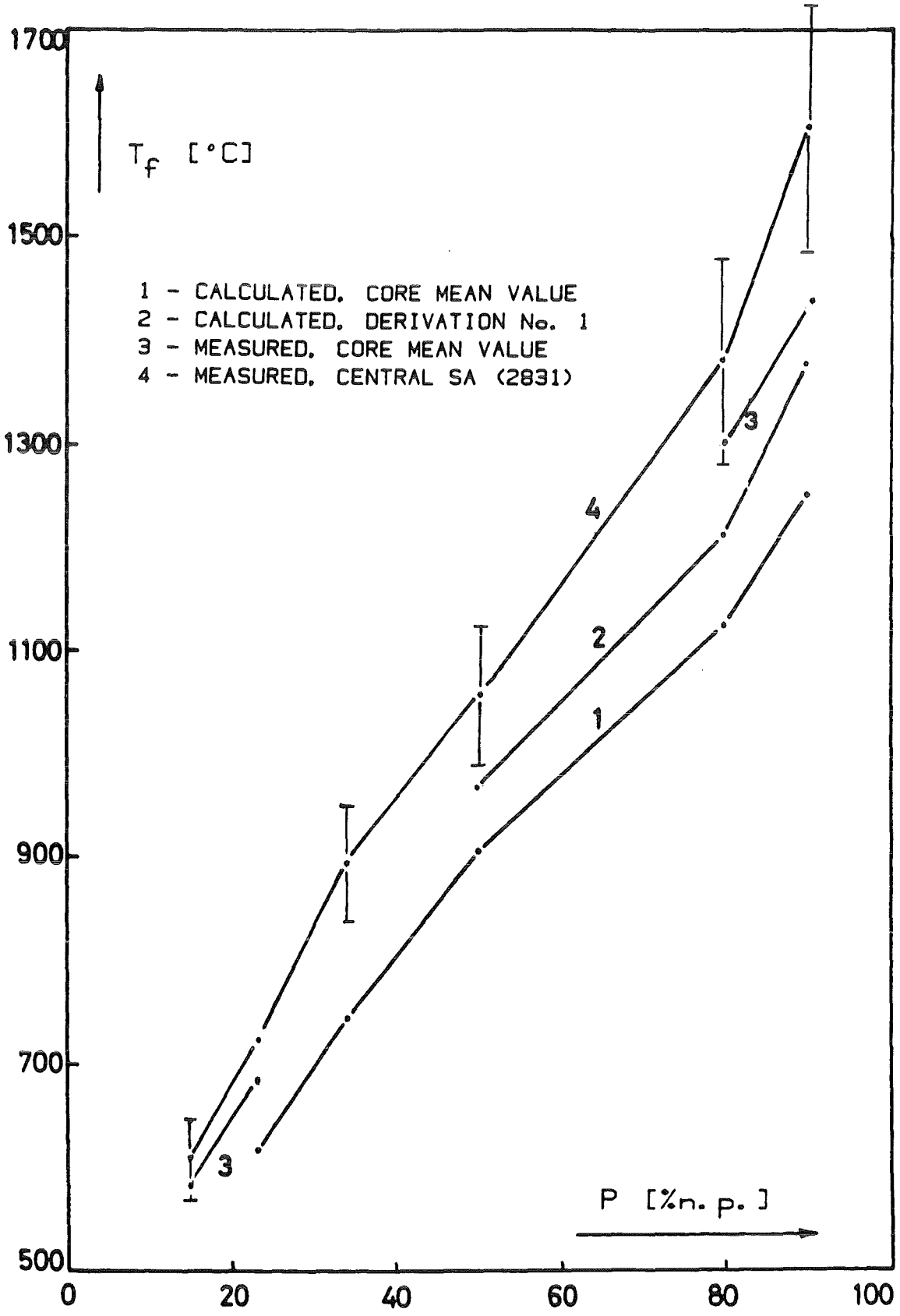

Fig. 18 Measured and calculated fuel temperatures versus reactor power

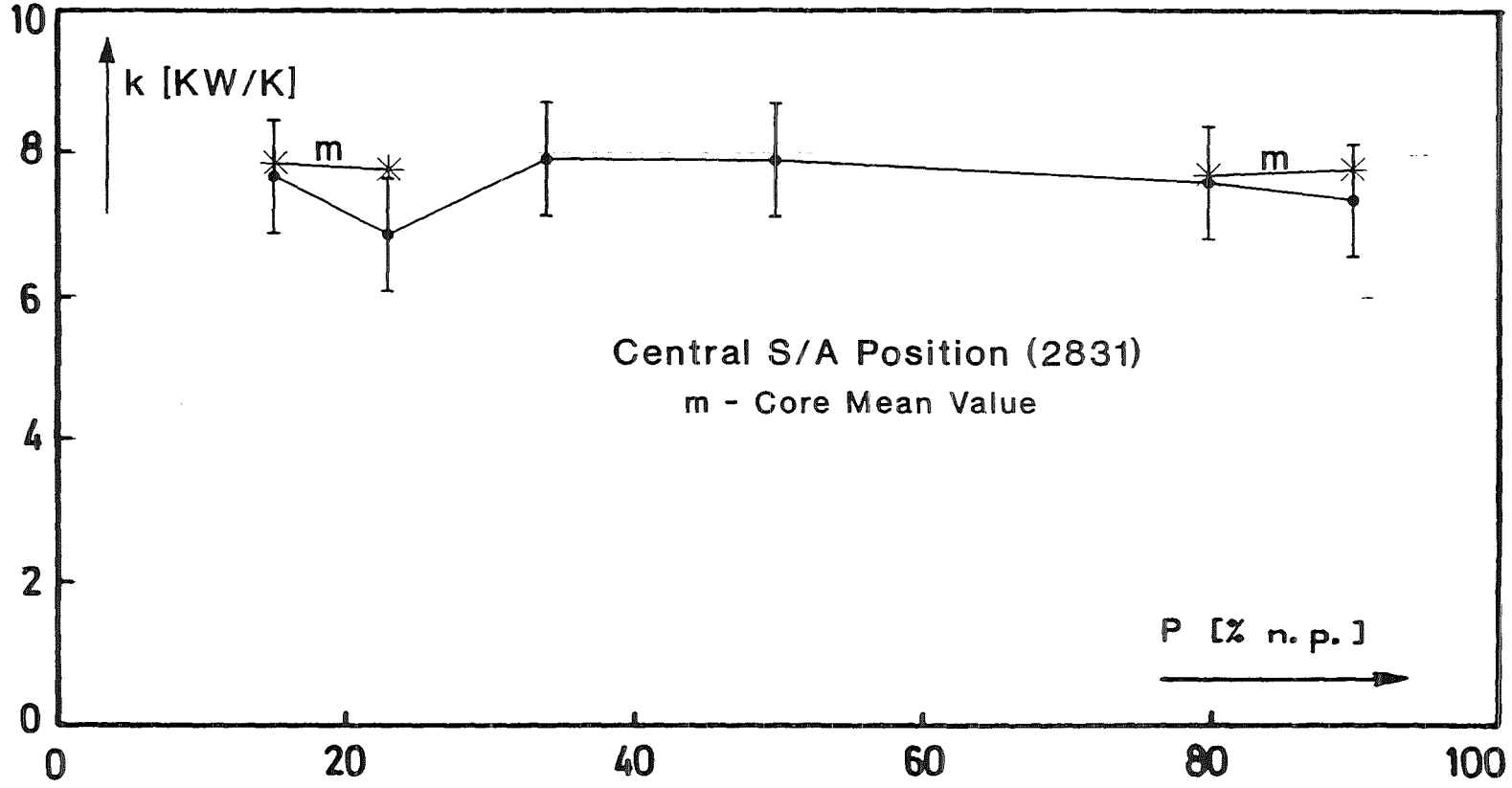

Fig. 19 Evolution of the SA heat transfer coefficient with power and burn-up

Symbols used in core maps: (Fig. 21-27)

I - Signal or SA index ($1 \leq I \leq 469$)

REP G - SA position coordinates (repères géographiques)

P - After SA position : core periphery

DT.Na - Coolant temperature rise (ΔT_c°, [°K])

DT.Fu - Fuel temperature rise ($T_f^\circ - T_c^\circ$, [°K])

TC.Fu - Fuel time constant (τ_f, [s])

TC.SA - SA time constant ($= Q_m/P^\circ$, [s])

DT.Rs - Residual coolant temperature rise ($\Delta T_c(t = 40\ s)$)

SA P. - SA power (P°, [KW])

TM.Fu - Mean fuel temperature (T_f°, [°C])

To.Na - Coolant outlet temperature (T_o°, [°C])

Koeff - Heat transfer coefficient (k, [KW/°K])

MF.Na - Coolant mass flow rate (F, [Kg/s])

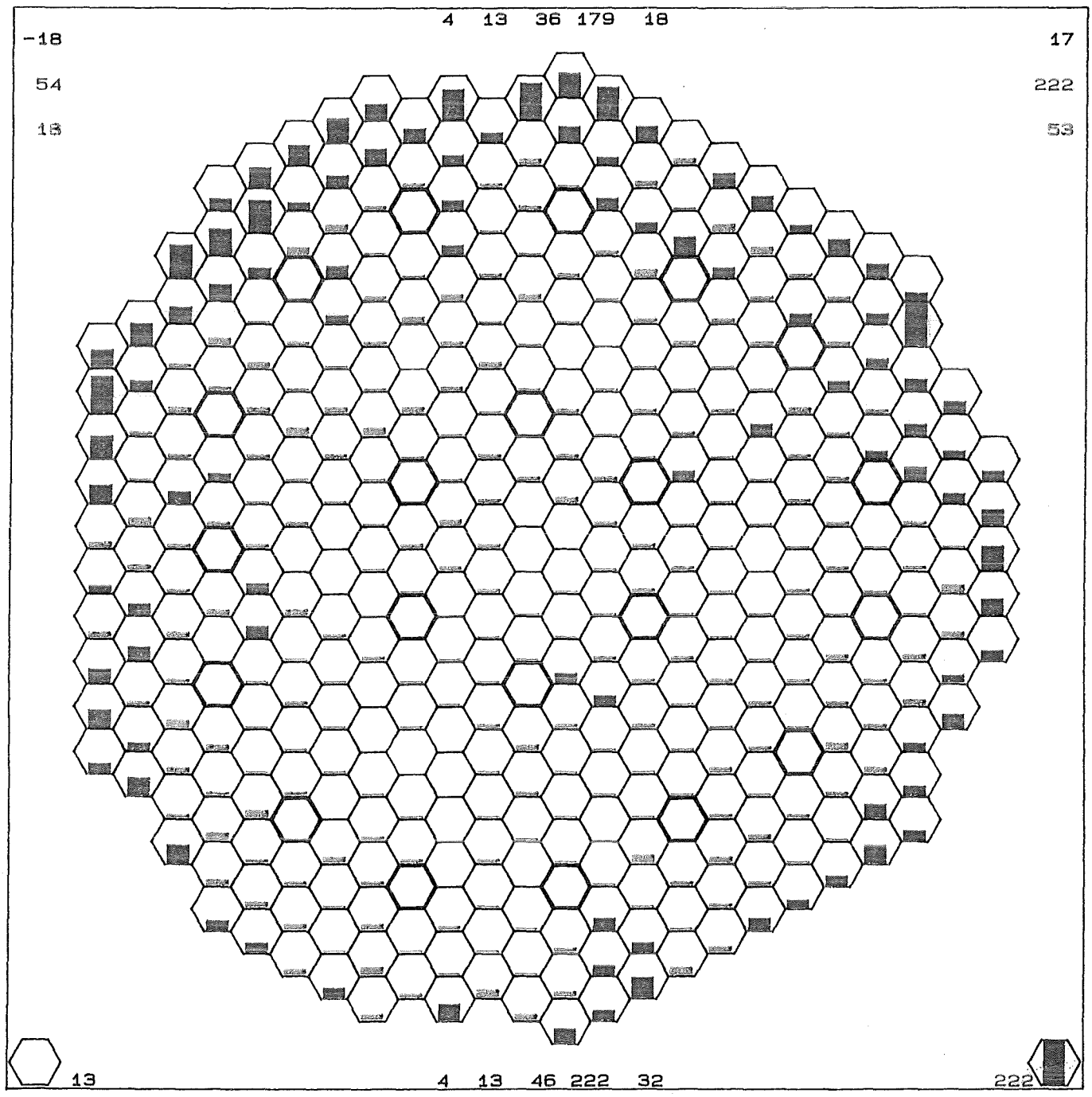

Fig. 20 Standard deviation of SA outlet temperature fluctuations at 90% n.p.

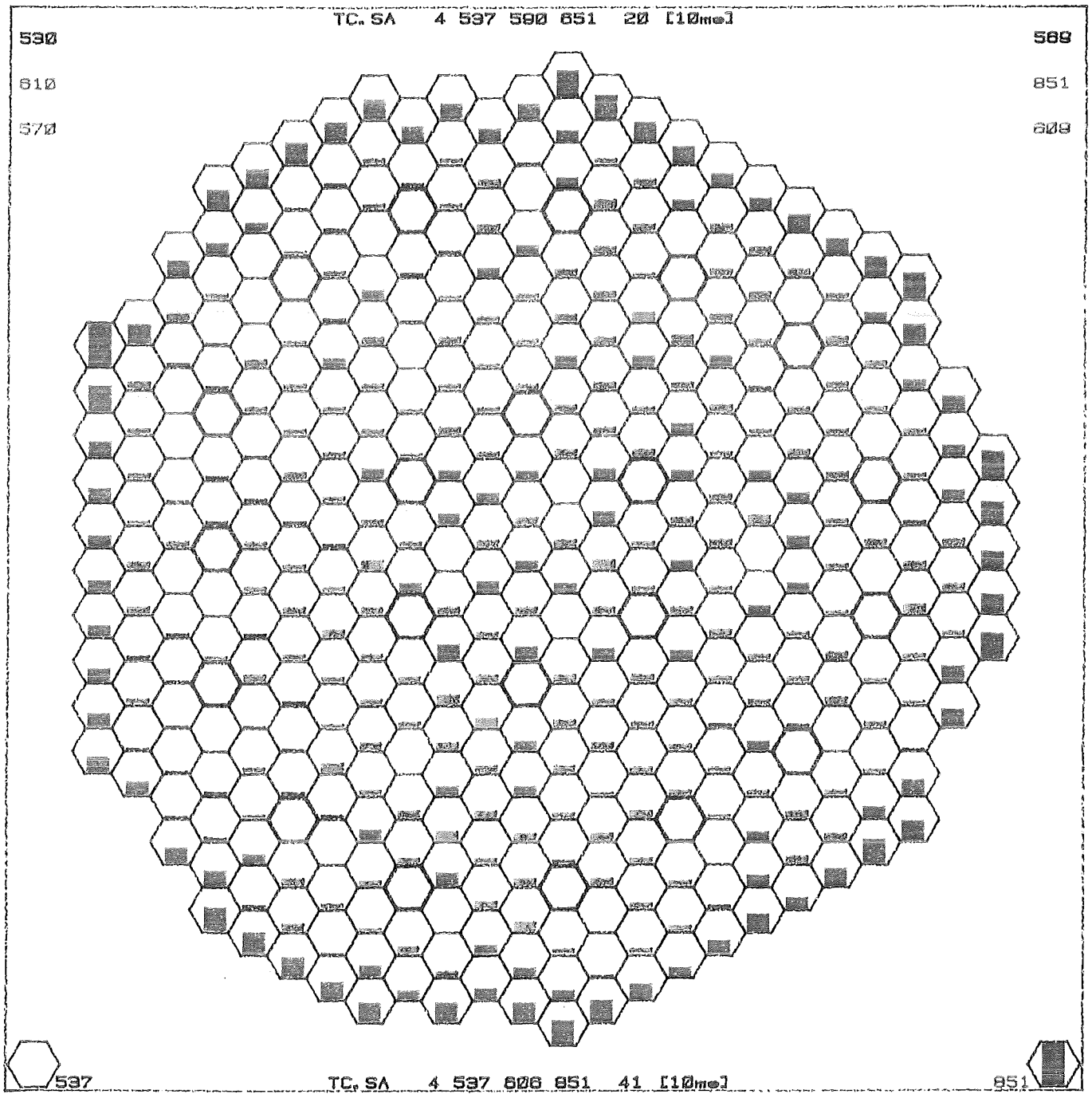

Fig. 21 Whole SA time constants at 90% n.p. and nominal flow

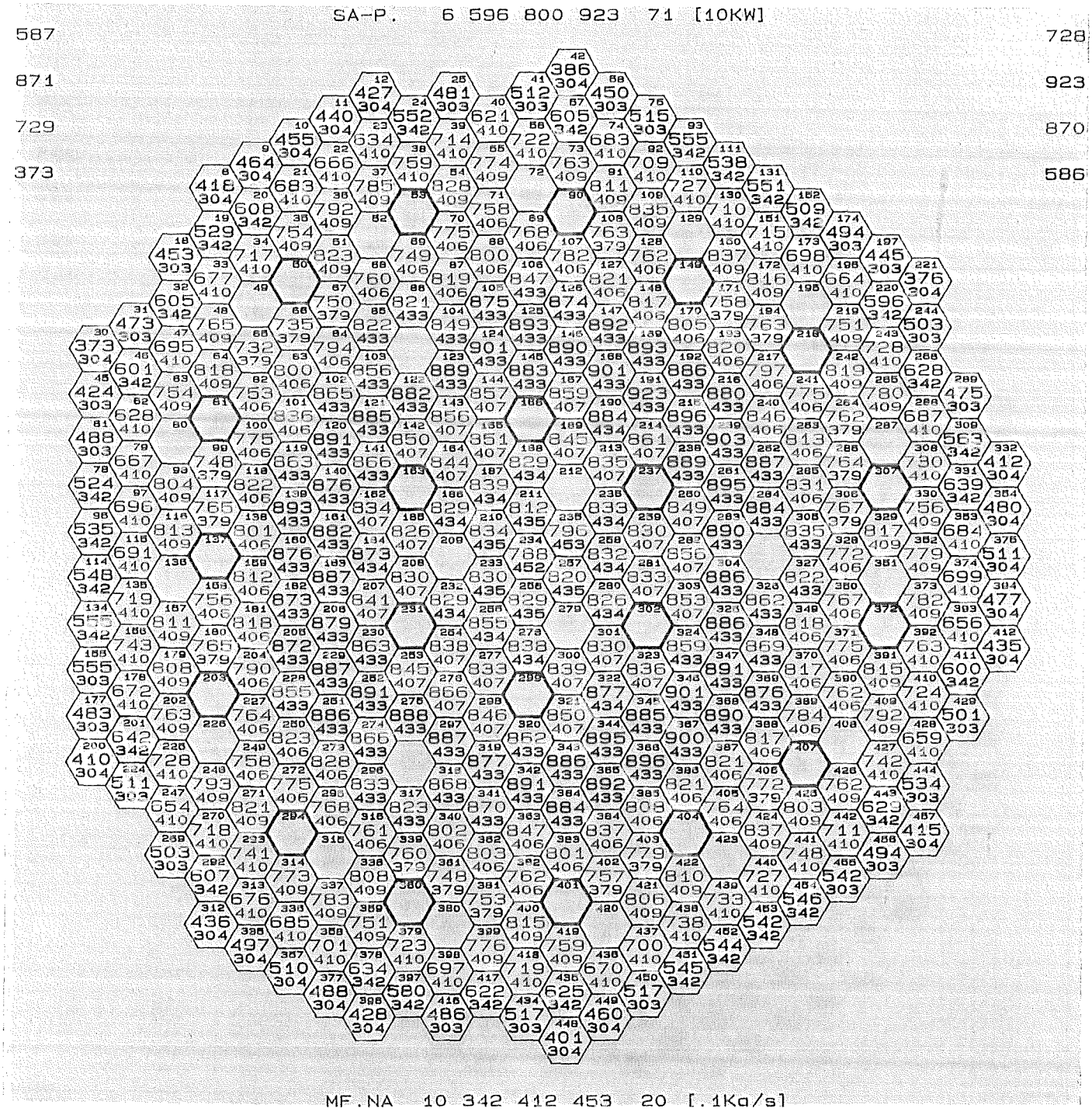

Fig. 22 SA power and coolant flow rate at 90% n.p. and nominal flow

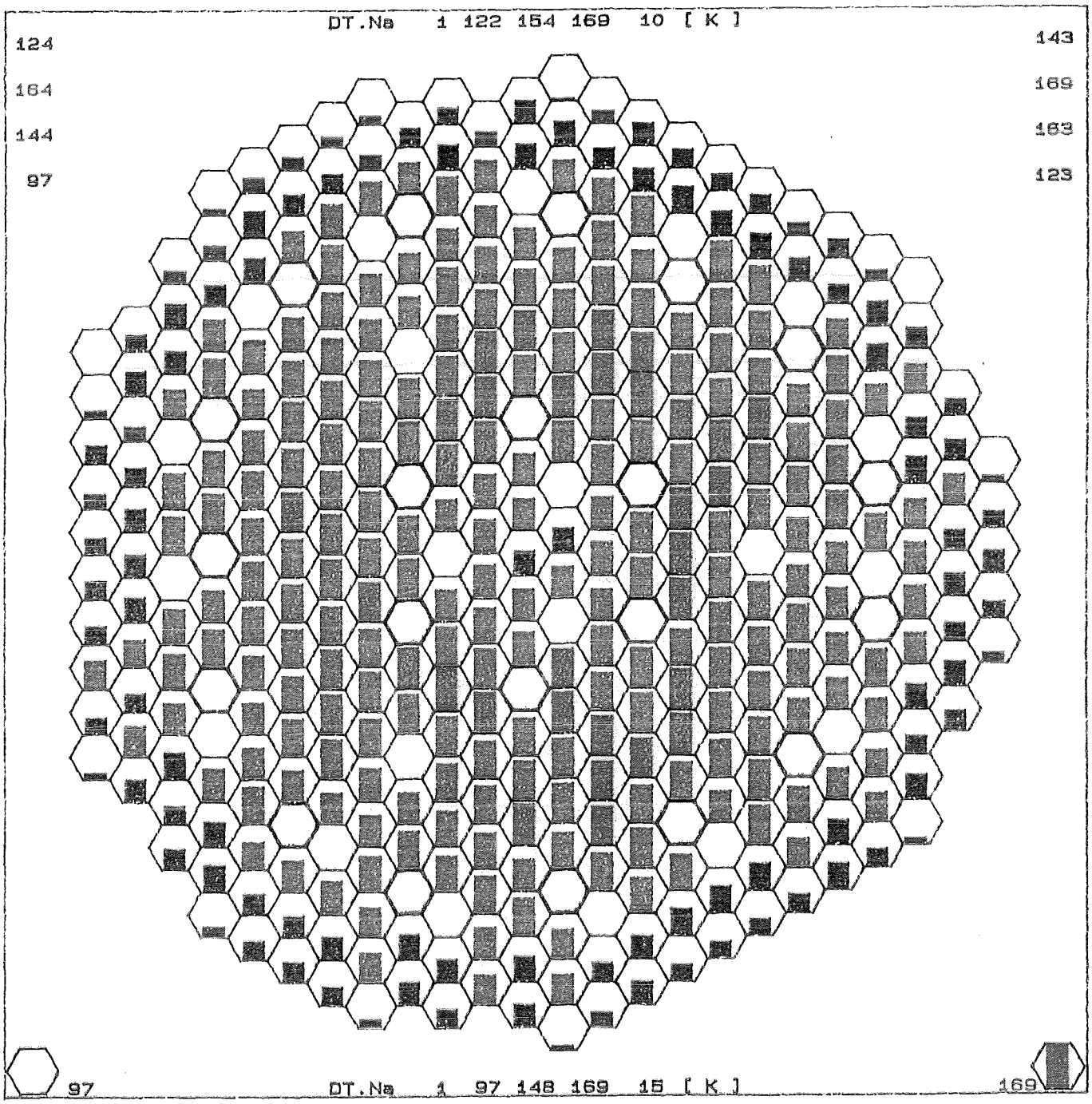

Fig. 23 SA coolant temperature rise; 90% n.p., full flow

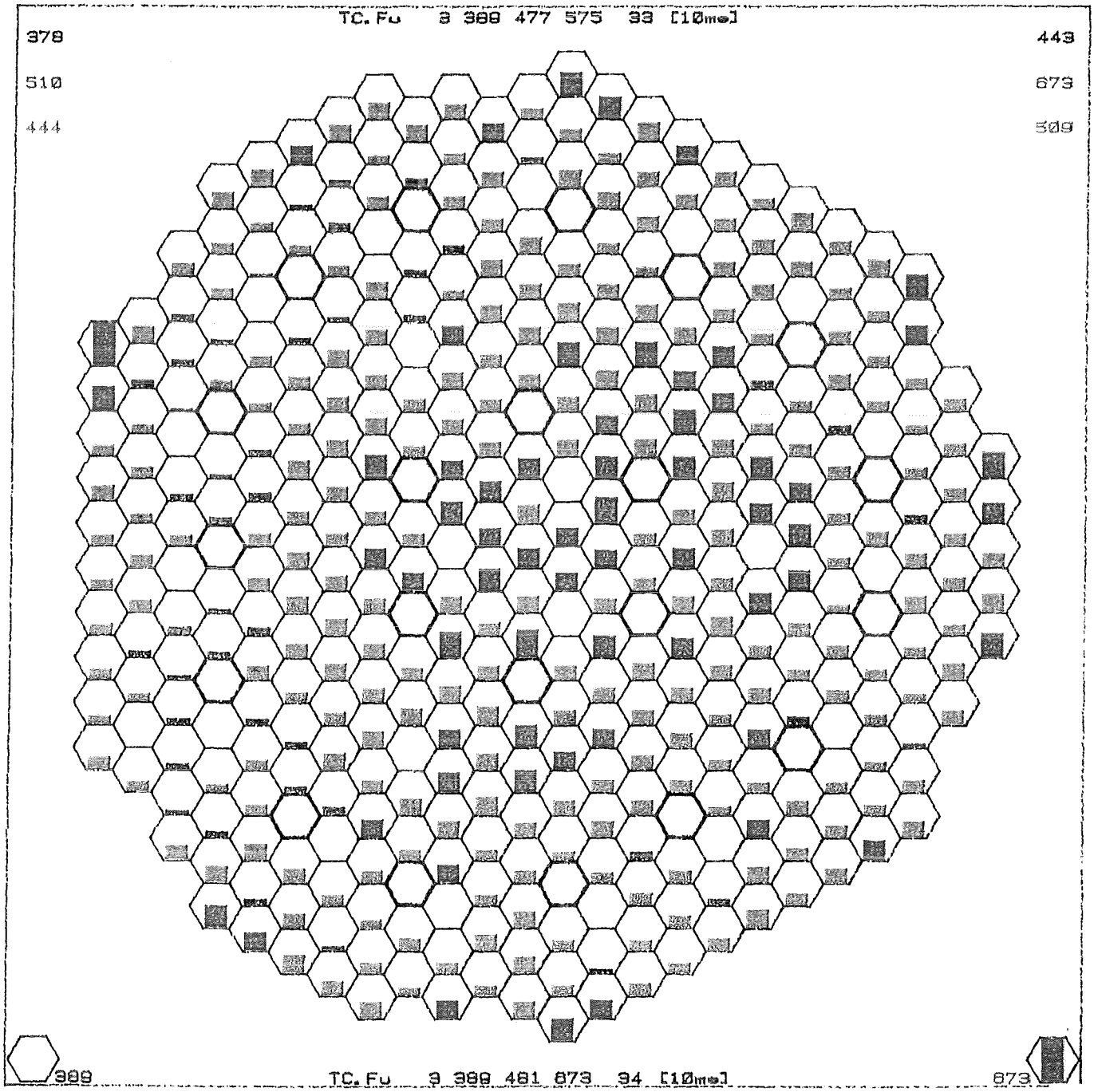

Fig. 24 Fuel time constants; 90% n.p., full flow

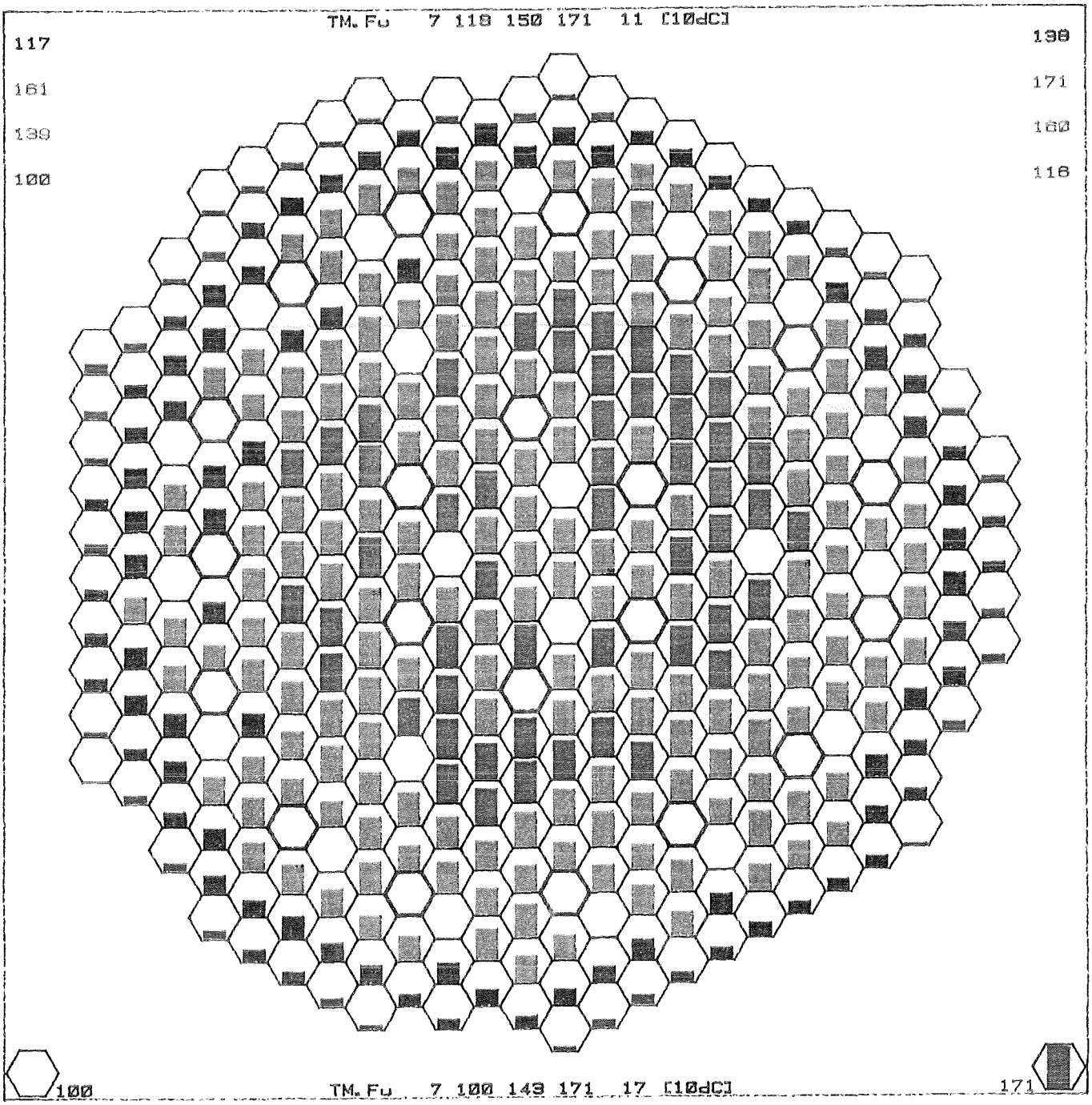

Fig. 25 Mean SA fuel temperatures; 90% n.p., full flow

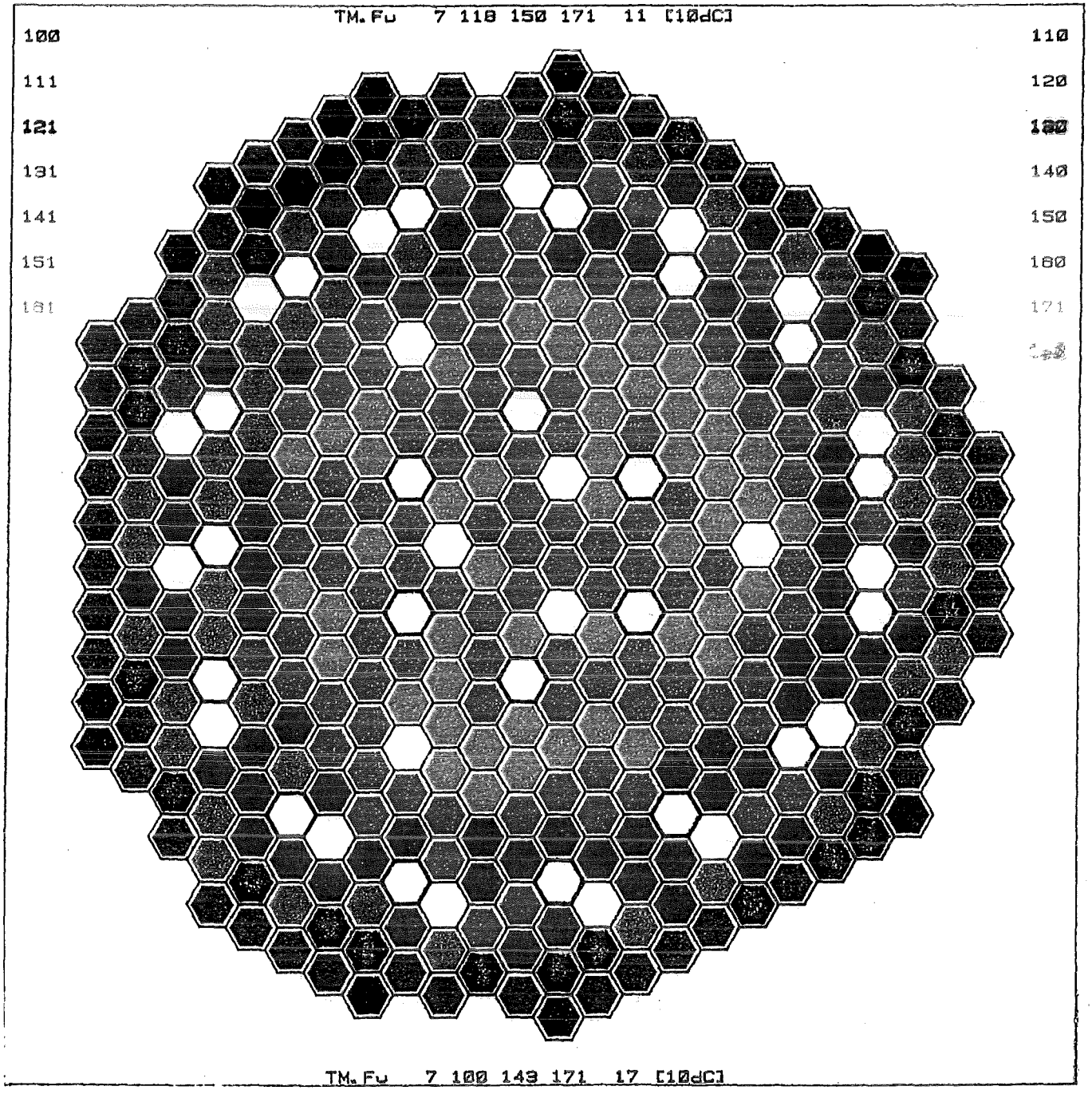

Fig. 26 Mean SA fuel temperatures; 90% n.p., full flow

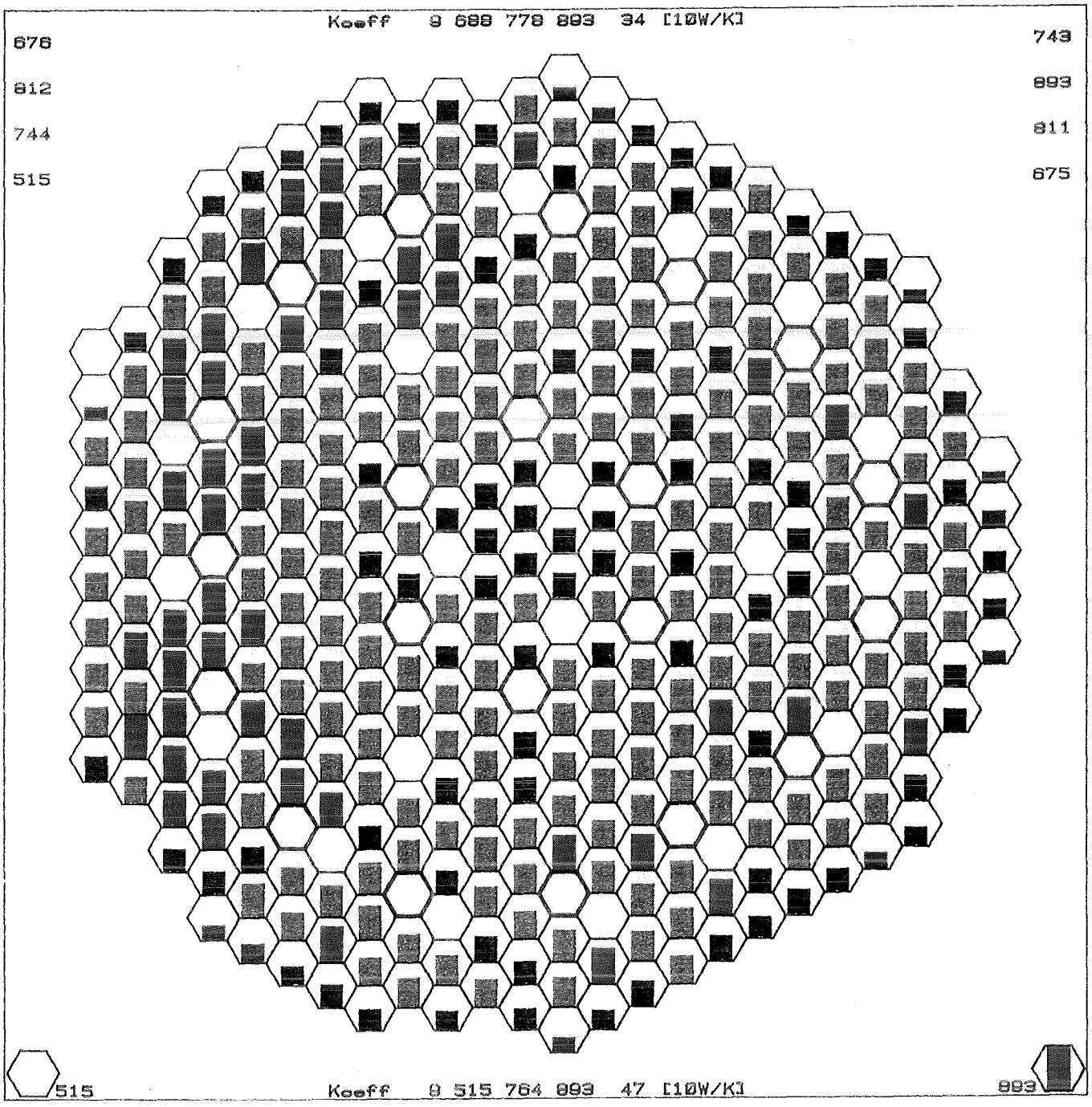

Fig. 27 SA heat transfer cefficient between fuel and coolant; 90% n.p.

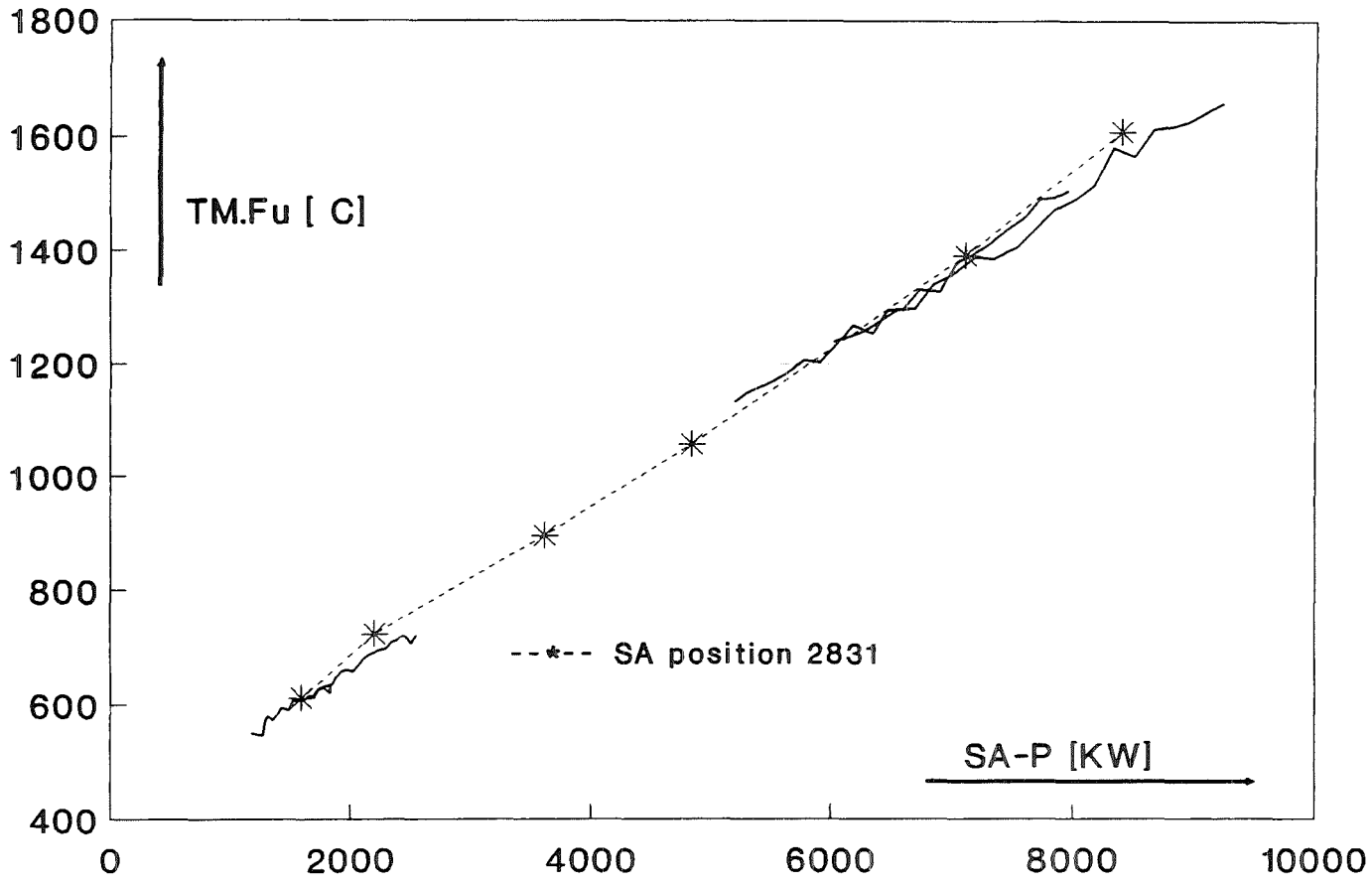

Fig. 28 Mean SA fuel temperature as a function of SA power

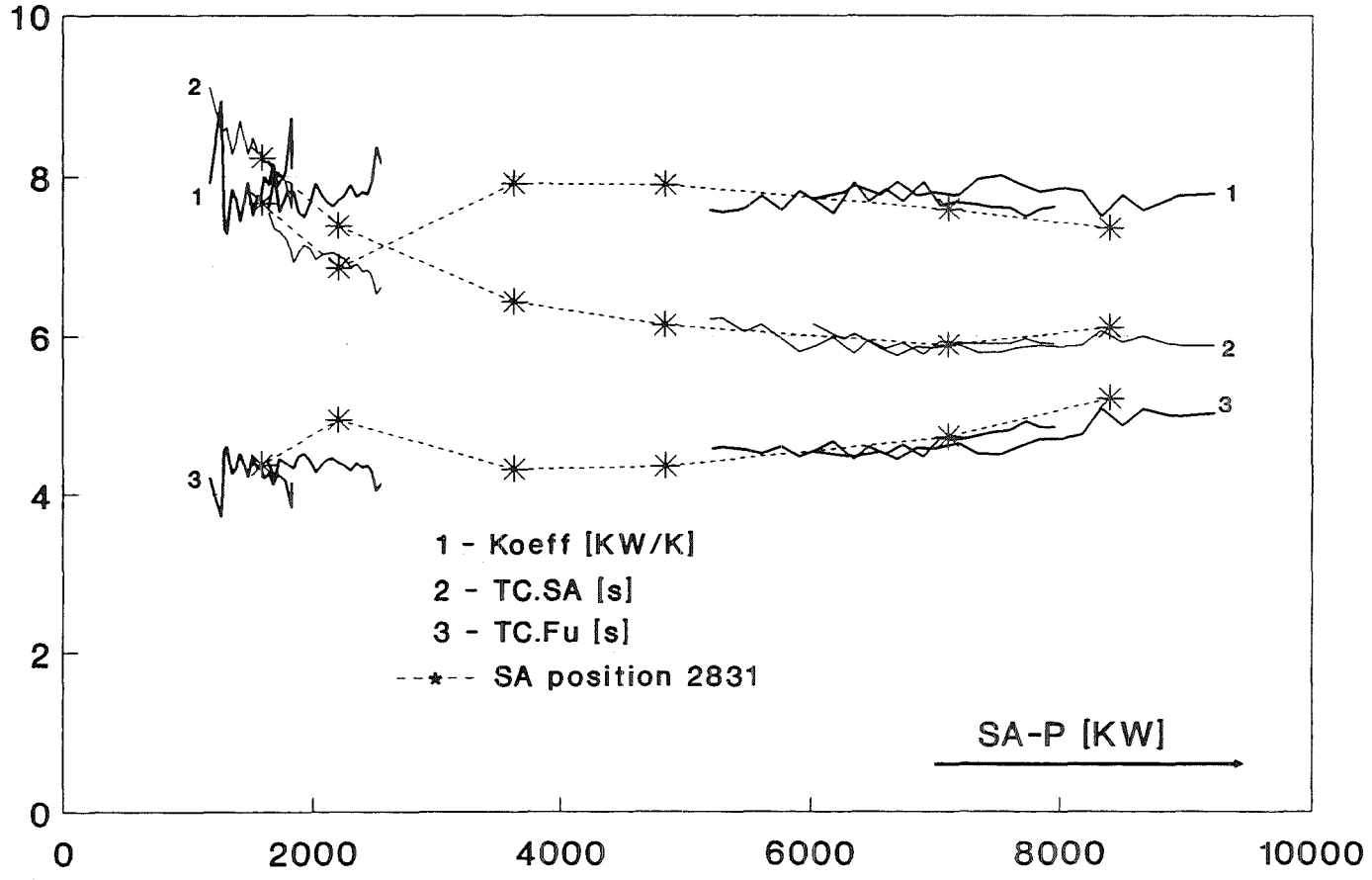

Fig. 29 Whole SA and fuel time constants and heat transfer coefficient as a function of SA power

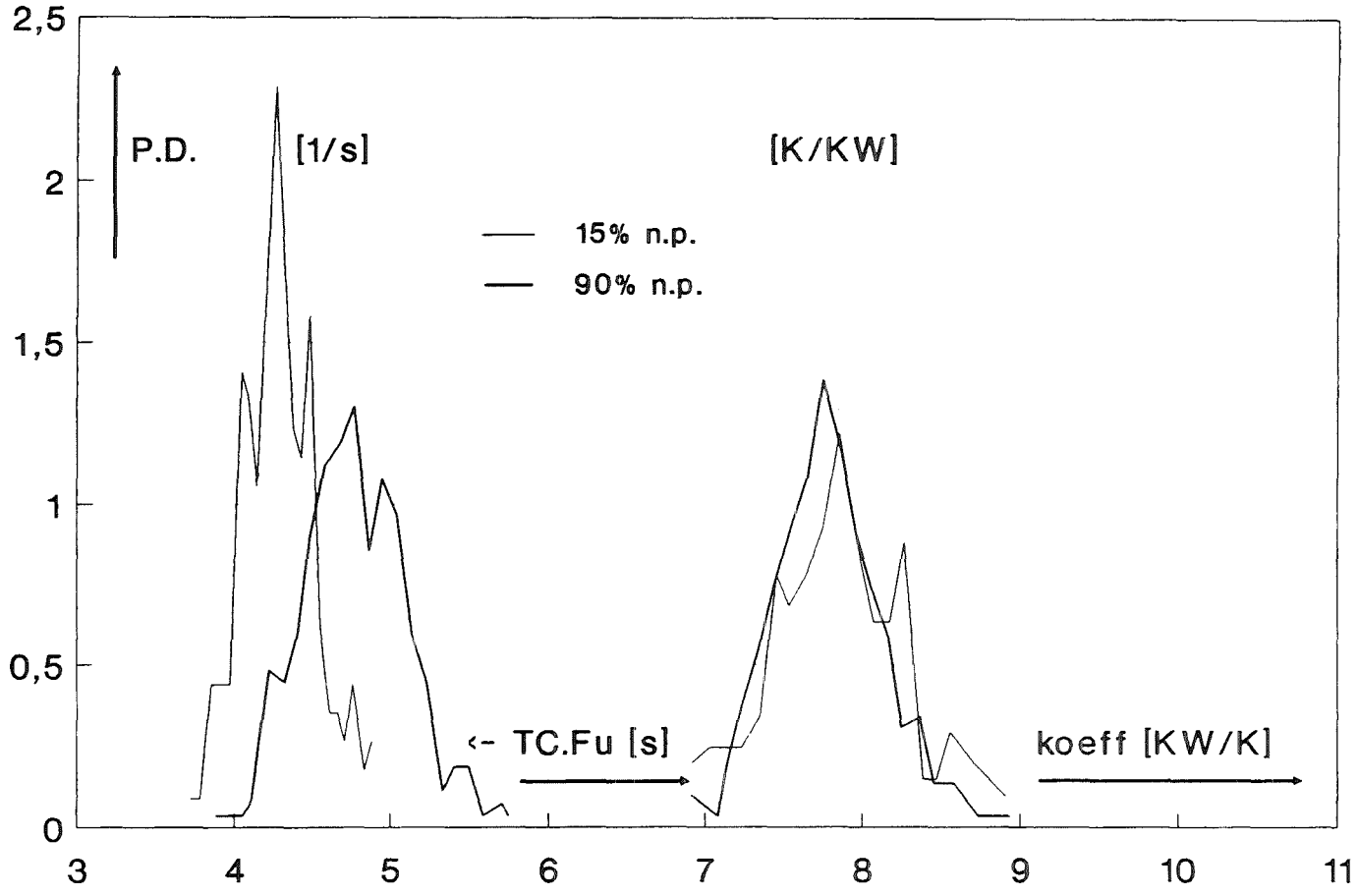

Fig. 30 Probability density functions of
fuel time constant and heat transfer coefficient